



GEANT4 SIMULATIONS OF THE
MÜNSTER DUAL PHASE XENON TPC

GEANT4-SIMULATIONEN ZUR
MÜNSTERANER 2-PHASEN XENON-TPC

BACHELORARBEIT

Lutz Althüser

Westfälische Wilhelms-Universität Münster

Institut für Kernphysik

AG Prof. Dr. C. Weinheimer

Themensteller: Prof. Dr. C. Weinheimer

Zweitgutachter: Prof. Dr. J. Wessels

Münster, September 2015

Contents

1	Introduction	1
2	The Muenster dual phase xenon time projection chamber	3
2.1	Detector geometry and functionality	3
2.2	Light collection efficiency and light yield	5
2.2.1	Calibration sources and positioning	7
2.2.2	Gamma interactions	8
3	Monte-Carlo simulations of the Muenster time projection chamber	11
3.1	GEANT4	11
3.1.1	Detector geometry	12
3.1.2	Particle tracking and basic detector response	14
3.2	Scintillation light propagation	16
3.2.1	Light collection efficiency	16
3.2.2	Light yield	21
3.3	Calibration simulations of the Muenster time projection chamber	25
3.3.1	^{57}Co	26
3.3.2	^{60}Co	29
3.3.3	^{137}Cs	33
3.3.4	^{83m}Kr	37
4	Conclusion and outlook	41
	Bibliography	43

1 Introduction

Since the postulation of the concept of dark matter in the 1930s, more and more evidence for dark matter, such as astronomical observations, have been found and several theories have been developed in order to characterize it. However, none of these theories could be verified by an experimental detection so far, which makes it an interesting field of research. Most of these experimental setups look for a special class of theoretical particle, the Weakly Interacting Massive Particle (WIMP).

One of these dark matter experiments following the path of detect WIMPs is the XENON Dark Matter Project, which is an international research project operating in the deep underground of the Laboratori Nazionali del Gran Sasso (LNGS) in Italy. The used detector, a dual phase xenon Time Projection Chamber (TPC), searches for WIMPs by looking for recoil signals. This detector setup, a combination of xenon as detection material and the dual phase concept, provides a high sensitive experiment for detecting WIMP-nucleon cross sections. The already operating development step, XENON100, which contains about 160 kg of liquid xenon, will be followed by the XENON1T detector, which further increases the sensitivity by 2 order of magnitudes.

In order to investigate and test new systems for these experiments, as well as doing further studies of a similar detector setup in Muenster, a smaller scale TPC was built in 2011. This dual phase xenon Muenster TPC can be operated in the same way as the full scale experiments. For the calibration of the dual phase TPC experiments regarding its light yield (LY) and light collection efficiency (LCE), radioactive sources can be placed near the detector. The penetration of these sources depends on the inner volume of the detector, due to the self shielding effect of xenon, and on the used materials.

The aim of this bachelor thesis is to investigate whether the available radioactive calibration sources can reach the entire detection volume or whether an alternative method, like an internal low energy calibration, can be used. In order to do this, a simulation package of the Muenster TPC was developed, and different calibration scenarios have been tested. After an introduction to the Muenster dual phase xenon TPC and GEANT4, the scintillation light propagation and the impact of different parameters on it, as well as LCE and LY map, will

be shown. Following this, the calibration possibilities of four different radioactive sources for the Muenster TPC will be presented.

2 The Muenster dual phase xenon time projection chamber

A typical time projection chamber (TPC) consists of a cylindric gas-filled detection volume, which is located in an electric or in some cases magnetic field, which can be applied to minimize the diffusion of electrons from ionization of the gas. The electric field is applied to drift the electrons to one side of the detector. This setup of a TPC allows to determine the primary position of the produced electrons.

2.1 Detector geometry and functionality

The Muenster dual phase time projection chamber is a TPC which uses liquid xenon with a gaseous phase on top as active volume to detect scintillation and ionization signals (see [10]) created inside the liquid xenon by incoming particles.

This dual phase xenon TPC consists of a cylindrical volume with a height of 170 mm and 80 mm diameter made of polytetrafluoroethylene (PTFE), better known as Teflon[®]. PTFE is chosen due to its high reflectivity for 178 nm photons, which are generated by interaction of different particles with liquid xenon [5]. The top and bottom of the detector volume is equipped with a total of 14 photomultiplier tubes (PMTs) for the detection of scintillation light. These photomultiplier tubes detect weak light signals due to the photoelectric effect, where electrons, called photoelectrons (pe), are emitted from a bialkali cathode due to the irradiation of photons, and amplified to a detectable signal.

Incoming particles induce electron (photoexcitation and photoionisation) or nuclear recoils in the xenon and produce scintillation and ionization signals. The scintillation signal (S1) produced in the liquid volume is mainly reflected at the surface of the liquid xenon and detected by the bottom PMTs. Due to two externally applied electric fields, the electrons from the ionization drift along the 17 cm chamber until they reach the gas phase and are extracted into it by the second field. The first electric field from the bottom mesh, as shown in figure 2.1, set to negative potential (cathode), to the central mesh, set to ground (gate mesh), is called the drift field E_{drift} and has an electric field strength of 1 kV/cm. The second

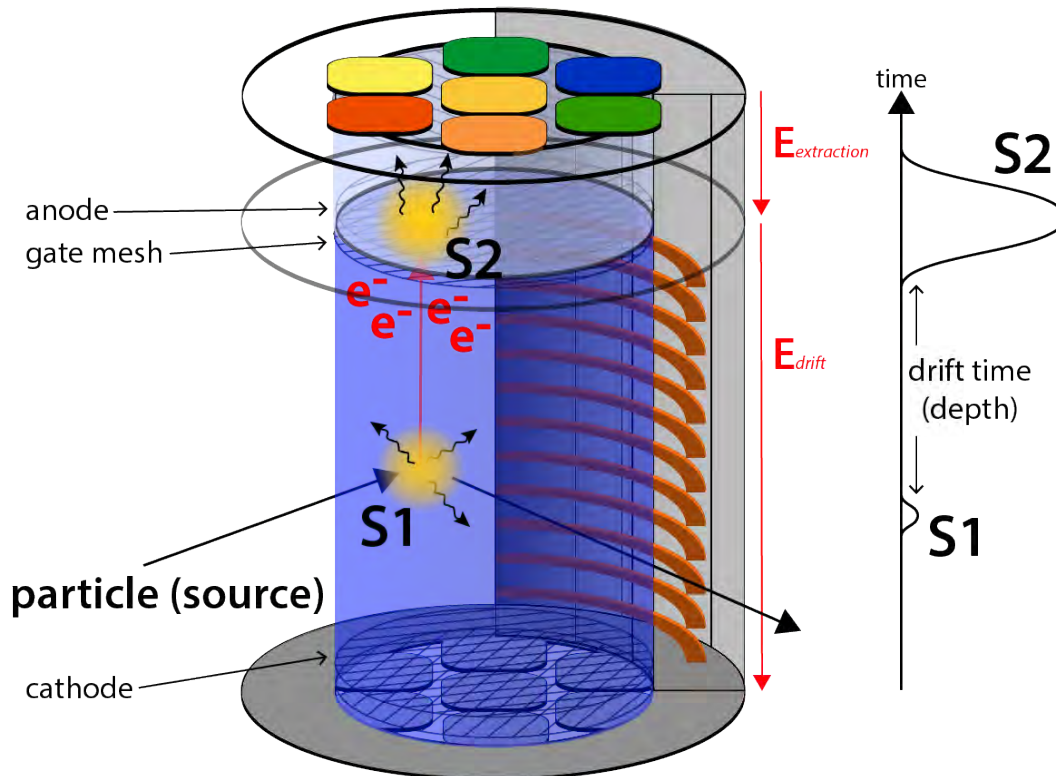


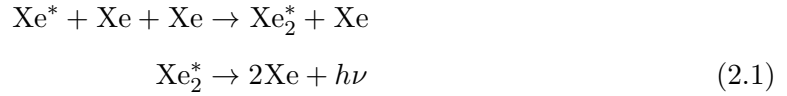
Figure 2.1: Sketch of the working principle of the Muenster dual phase xenon time projection chamber. The origin of the S1 (scintillation) and S2 (scintillation due to ionized electrons) and the impact on the top PMT pattern are shown. The dimensions do not represent the real detector in every detail.

electric field, applied between gate mesh and top mesh, set on positive potential (anode), is named extraction field $E_{\text{extraction}}$ and has a field strength of 8.8 kV/cm . In order to protect the PMTs, two additional meshes are installed in front of each PMT pattern (see figure 2.1). The electrons in the gas phase are accelerated by the extraction field and produce a second scintillation signal, caused by interactions with xenon atoms in the gas phase (proportional scintillation), which is mainly collected by the top PMTs and is called S2 signal. The size of the S2 signal is directly proportional to the number of extracted electrons.

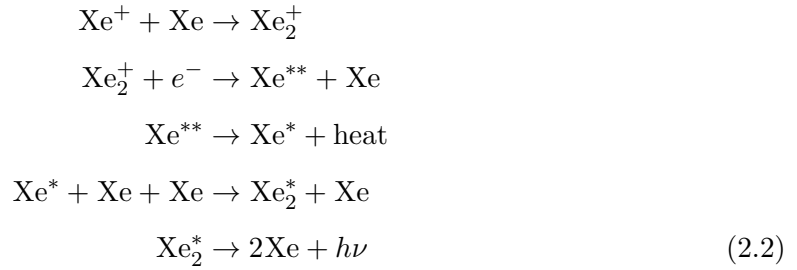
As outlined above, a position reconstruction can be realized using the dual phase TPC. The depth of the interaction location (z -coordinate) can be determined by the drift time of the electrons from the ionization (see figure 2.1). These electrons have a constant velocity of about $2 \text{ mm}/\mu\text{s}$ [5]. As visualized in figure 2.1, the PMTs are arranged in an cylindrical 2-3-2 array. Due to this, the x - and y -coordinates can be calculated out of the hit pattern of the top PMTs. The quality of this full 3D position reconstruction is limited to the number of PMTs in the top array. While the resolution of the x - and y -coordinates is usually defined by the PMT shape and patterns, the z -position of the interaction, depending on drift velocity and drift time, can be obtained with a resolution of a few millimeters.

Scintillation and ionization process

According to [5], the scintillation process of xenon consists of different reactions. Put simply, the scintillation light is emitted by an excited xenon dimer state (Xe_2^*) decaying to the ground state. This excitation state can be created in two different simultaneous reactions. The first reaction starts with an excited xenon atom, produced after scattering process with the incoming particle, as the initial condition.



The second reaction is a collection of several reactions following an initial ionization:



As seen in these scintillation reactions, it can be outlined that xenon is transparent for its own scintillation photons since the produced photons are emitted by an excited dimer state, so that the scintillation light is not absorbed by other xenon atoms. The average required energy to produce one scintillation photon in liquid xenon is $W = (21.61 \pm 0.21) \text{ eV}$ [11].

By applying the electric drift field, the second line in the reactions in equation (2.2) is suppressed and a part of the produced electrons is separated from the ions, thus missing for the recombination process. Due to the amplification of the ionization signal by the electric field the S2 signal is always much larger than the S1. With the ratio of S_2/S_1 , which is always smaller for nuclear recoils than for electronic recoils, it is possible to perform a background discrimination of the electronic and nuclear recoil [5].

2.2 Light collection efficiency and light yield

As explained previously, the working principle of the Muenster dual phase xenon time projection chamber is based on detecting scintillation light from interactions of particles with liquid xenon and accelerated electrons in the gaseous phase. According to this principle, the detection of light is one of the most important part of the detector setup. This light collection, obtained as PMT hits, depends on the amount of photons of the S1 and S2 signal.

The amount of photons can be affected by the recoil energy produced in scattering processes as described in section 2.1 as well as by the primary position of the scintillation signal in the TPC. This effect can be described by the light collection efficiency (LCE) [7], which is the percentage of photons that reaches the PMTs out of a given position in the detection volume relative to the amount of initial photons. The number of detected photons depends on the attenuation length in liquid xenon or other detector materials, the limited reflectivity of PTFE and the limited efficiency of the PMTs, as well as the position of interaction due to different solid angles. The attenuation of the photons is defined by its absorption length and is a function of the purity of xenon.

To fully understand the detector geometry, not only the average LCE of the entire detection volume is important, but in particular the LCE map, which is the position dependent definition of the LCE for a given amount of volumes in the TPC, needs to be known. With the LCE map it is possible to obtain the deposited energy on each position in the TPC. The LCE, as well as the LCE map can only be obtained by simulations, thus the amount of initial photons is known.

In figure 2.2 the relative LCE map for the XENON100 TPC is shown. A relative LCE is calculated by the ratio of the local LCE to the average LCE in the detector and is used to

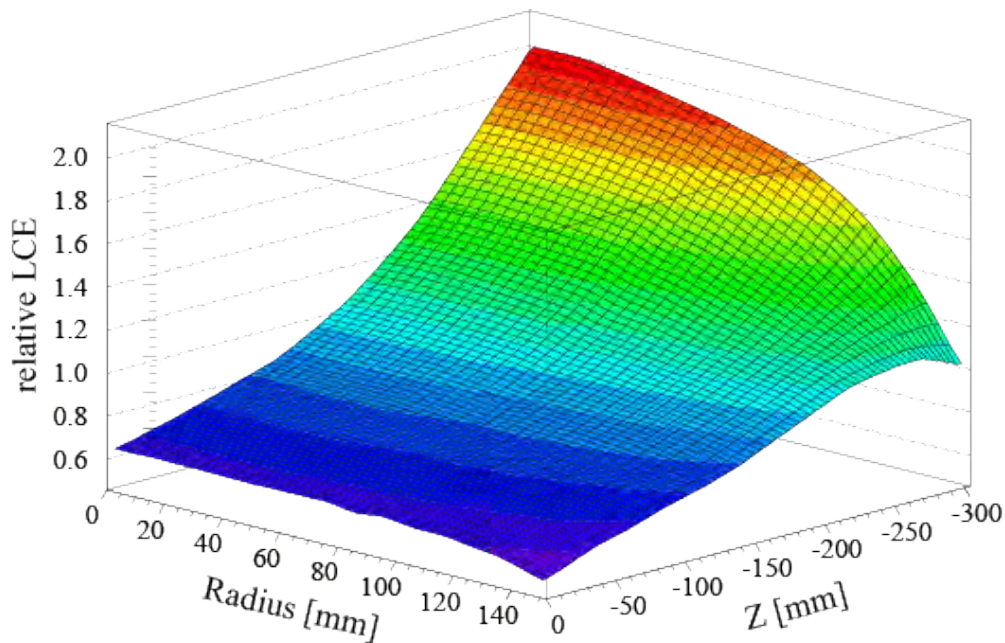


Figure 2.2: Light collection efficiency correction map for the XENON100 detector obtained from the 40 keV line. The relative light collection efficiency is given by the ratio of the local LCE to the average LCE in the detector. The vertical axis shows the value to correct a measured S1 (light) signal at a given (r, z) position. $z = 0$ mm denotes the top of the TPC. The measured S1 signals are divided by the values from this map.[7]

correct the detected signal in processes, where the total amount of photons is unknown, such as for non-simulation applications. As seen in figure 2.2 the relative LCE is on the bottom ($z = -300$ mm) of the TPC much higher than at the top, and a radius dependency is given. This is caused by the liquid xenon surface, which reflects photons and thus increases their path.

In order to be able to measure a signal of interest just above the background signal level, the light collection must be as good as possible. Using the relative LCE map it is possible to correct the given S1 signal, so that for a specific recoil energy the corrected S1 signal is the same for positions in the top or in the bottom of the TPC. Thus, the energy can be calculated for every position in the TPC in the same way. Due to the detector symmetry, the light collection efficiency needs only be done in dependency of r and z (see figure 2.2).

Final the assigned energy to the actually detected photon signal is the light yield (LY) [7], which can be defined as the number of collected photoelectrons per keV recoil energy. This can also be described as the light collection efficiency combined with the light collection or signal as the number of S1 photons per keV of deposited energy. It is notable that the LY is energy dependent.

2.2.1 Calibration sources and positioning

The LCE for the Muenster time projection chamber can be obtained with a mono-energetic gamma source. With this mono-energetic source and the 3D reconstruction it is possible to determine the relative LCE of each event. Additionally an average LY can be calculated. Events in which the full gamma energy has been deposited in a single scattering site have a known recoil energy. This recoil energy is equal to the incident gamma energy and can be used to select these special events.

Therefore, some considerations have to be taken into account when choosing the optimal calibration source for different situations. Due to a density of liquid xenon of about 3 g/cm^3 and the high atomic number of 54, xenon provides a good self-shielding for γ -radiation. As a consequence of this the possible sources have to penetrate the center of the TPC with a sufficient statistic. Therefore, a high energetic gamma source, which can overcome the insulating vacuum chamber, the cryostat vessel and the self-shielding properties of xenon, is a possible candidate. Other radiation like alpha and beta particles are completely stopped by the vacuum chamber.

In order to obtain an uniform illumination of the detector volume, the gamma source has to be placed at different positions around the time projection chamber (see section 3.3). This positioning could be different for various sources and can vary in the z and azimuthal

directions. The different kinds of γ interactions, which can take place, are presented in the following.

2.2.2 Gamma interactions

Gamma sources can interact in three different ways in the detector (see figure 2.3): Pair production, photoelectric effect and Compton scattering. For example, pair production is forbidden for the 662 keV gamma of ^{137}Cs . The photoelectric effect happens about 10% of the time, and Compton scattering is the dominating process [8].

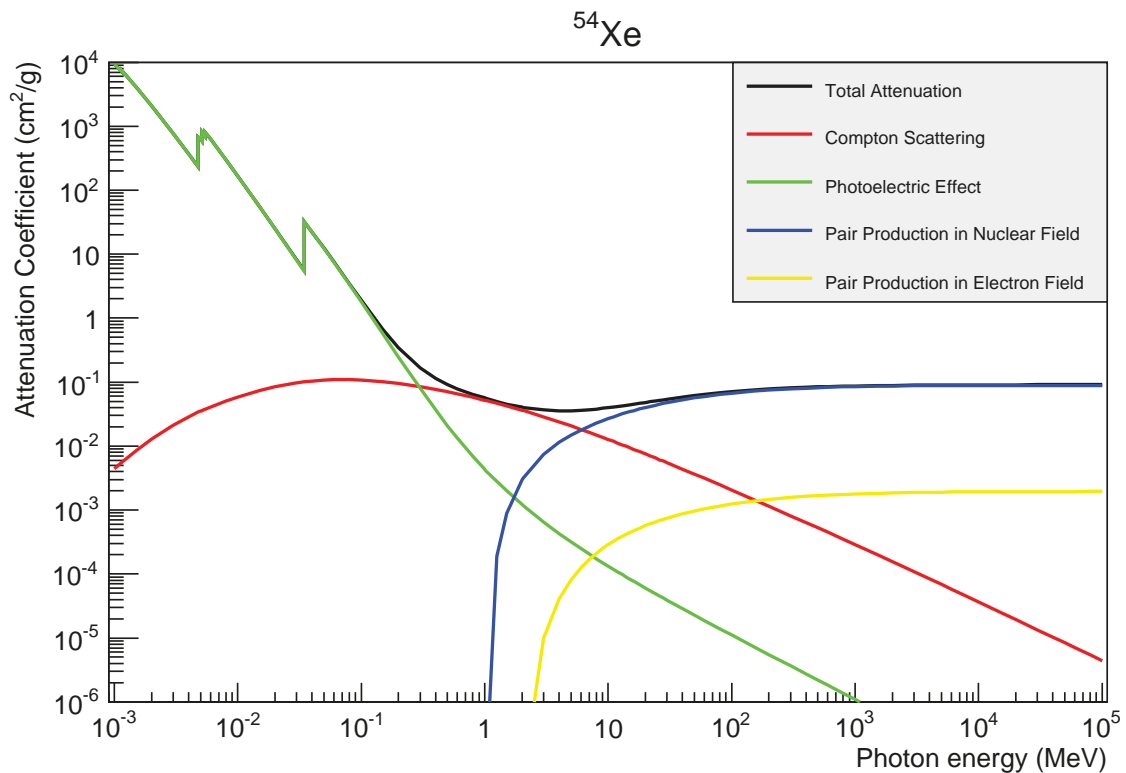


Figure 2.3: Attenuation coefficient in xenon for the photoelectric effect, Compton scattering and pair production.[3]

Pair production

As it can be observed in figure 2.3, pair production is the dominant interaction for gammas at high-energy above 6 MeV. In this interaction the energy of the gamma can be converted into an electron-positron pair near a atomic nucleus, which conserves the momentum of the initial gamma. Due this the nucleus receives some recoil.

Photoelectric effect

The absorption of a photon by an electron, where the photon energy is turned into the

ionization process, is called the photoelectric effect, which is a low-energy phenomena. The recoil energy of this light matter interaction E_{recoil} is less than the assumed energy of the incident photon E_γ . Due to the binding energy of the atom E_B , the interaction can be described by $E_{\text{recoil}} = E_\gamma - E_B$. In addition, the binding energy of the ionized electron is released into the detector volume as well, due to transitions of the ionized xenon-like x-ray emission and Auger electrons. Consequently, the full incident photon energy is deposited.

Compton scattering

The inelastic scattering of a photon off charged particles is called Compton scattering. In this case, the scattering of a photon with an electron is described. Due to energy transfer from the photon to the electron, the electron is recoiled while the outgoing photon is emitted with a lower energy. Two different possibilities for this outgoing gamma can be named: First, the lower energy outgoing gamma can do multiple Compton scattering if its energy is high enough to scatter again. This series will end in absorption of the gamma by the photoelectric effect. Due to this, the full energy of the initial gamma is deposited in the detector and thus part of the spectrum. Second, the gamma can leave the detector after Compton scattering and will contribute to the spectrum in a different way.

For ^{137}Cs the probability that a second interaction of the initial scatter for a 662 keV photon happens in a small distance of 3 mm is 9%. Consequently, the remaining 91% of these photons are discarded or leave the detector [8]. If multiple scattering happens in a small z-range, these events are suitable for calibration purposes. Multiple scatter events which take place in a large z-range will produce two distinctly identifiable S2 signals and can be discarded.

As described above, the calculation of the light collection efficiency requires a full energy deposition in the TPC, which makes it necessary to understand the Compton scattering in the detector volume. This can be studied by simulating the geometry of the TPC and testing it in different situations.

3 Monte-Carlo simulations of the Muenster time projection chamber

In order to understand and characterize the Muenster TPC, Monte Carlo simulations are necessary. These simulations can be used to improve the design of the detector or compare the simulated data to real data in order to understand each part of the underlying physics. The Monte Carlo methods or Monte Carlo experiments are a class of algorithms that are based on randomized sampling to obtain a certain result. Monte Carlo simulations are often used for modeling systems with high degrees of freedom in which other mathematical methods are not suitable. For physics-related problems, some simulation toolkits based on the Monte Carlo algorithm have been developed.

3.1 GEANT4

The simulation toolkit which is used to model the Muenster TPC is GEANT4 (Geometry and Tracking) by CERN [1]. It is the first toolkit out of the GEANT series which uses object oriented programming in C++. GEANT4 is invented as a platform for “the simulation of the passage of particles through matter” [1]. The application areas include high energy physics, nuclear experiments, medical, accelerator and space physics as well as low energy physics in the newer versions.

Almost every facet of the detector can be implemented with this simulation toolkit. The simulation is divided into main parts such as handling the detector geometry, tracking particles, detector response, run management, visualization and an user interface. In the geometry, the user can implement a physical layout of the experiment by using basic polygonal shapes. These resulting volumes can be assigned with properties such as reflectivity or material specifications and are completed by defining relevant physical effects or interactions. Possible interactions and decay processes of particles through matter will be tracked. The detector response emulates how a real detector would respond to a particle passing through. Different experimental setups can also be tested by defining an adequate run management with possibilities to change some detector and source properties. GEANT4 offers a huge amount of

possibilities to visualize the defined detector geometry and different user interfaces for direct input.

The modeling of a detector normally starts by implementing its full geometry and assigning certain physical effects as described in section 3.1.1. This is already done for the simulation package adopted from [8], designed for GEANT4 version 9.1. With the updated GEANT4 Version 10.01, huge improvements of the toolkit for simulating low energy physics have been introduced. Thus, the current GEANT4 routines of the Muenster TPC needed to be updated within this thesis. For that the simulation package of the Muenster TPC was rewritten to match the new specifications. Classes such as the *PhysicsList*, which implement all physical interactions and definitions, are replaced as a whole. The new simulation package for the Muenster xenon time projection chamber is written for GEANT4 Version 10.01 with the version name *geant4-10-01* (5-December-2014) and ROOT Version 5.34.

3.1.1 Detector geometry

One of the most important part of the implementation of the simulation package is the detector geometry, which is defined in the class *DetectorConstruction*. In this class are all relevant parts of the Muenster TPC added in order to reproduce a full physical layout of the experiment. The simulated detector also has a 17 cm drift length with a radius of 40 mm for the detection volume. In order to do light yield and calibration studies, the main detector volume is implemented, as well as all 14 1-inch-squared PMTs and meshes.

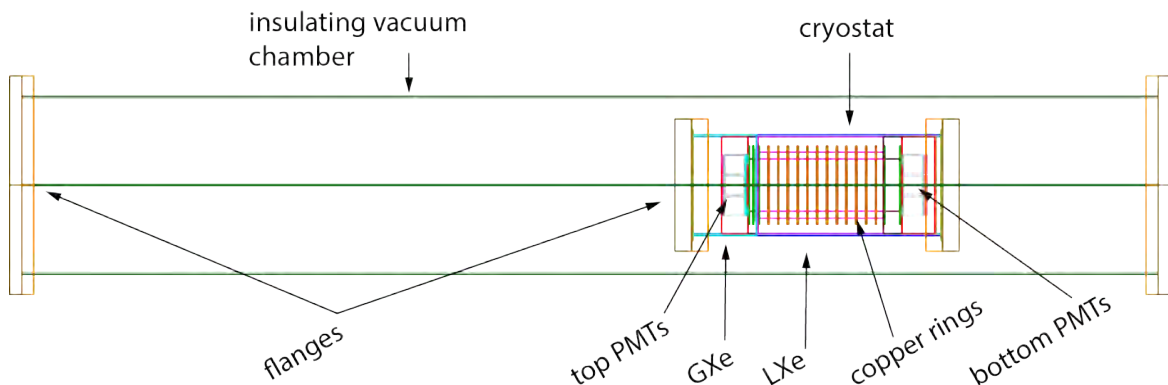


Figure 3.1: Visualization of the Muenster time projection chamber geometry with the *qt* visualization driver. The orientation of the TPC is rotated in order to get a better overview.

The insulating vacuum chamber is also fully included. This is necessary since possible calibration sources will be placed outside in the lab and have to pass through the stainless steel wall of the chamber, acting as a first interaction material. Consequently, the time projection

chamber and its inner cryostat are simulated in a high level of detail, neglecting feedtroughs and cabling. An overview of the simulated detector is pictured in figure 3.1.

Thus, the simulation package includes the vacuum chamber with flanges and the detector consisting of a inner cryostat, PTFE panels, electrodes and meshes, field shaping copper rings, PMTs, liquid and gaseous xenon. The parts are implemented considering all different materials and possible physical processes.

The photomultiplier tubes are built out of six different volumes as shown in figure 3.2. Each volume is confined to another, defined by a material and composited to a single photomultiplier tube. A PMT consists of a quartz window based on a steel casing. In this case, an aluminium photocathode¹ and vacuum volumes are placed. These volumes merged as one simulated PMT begin working by defining the ability to collect PMT hits to the photocathode and defining the used materials. Defining a material can be done by adding all of its elements and densities or by using the default predefined materials.

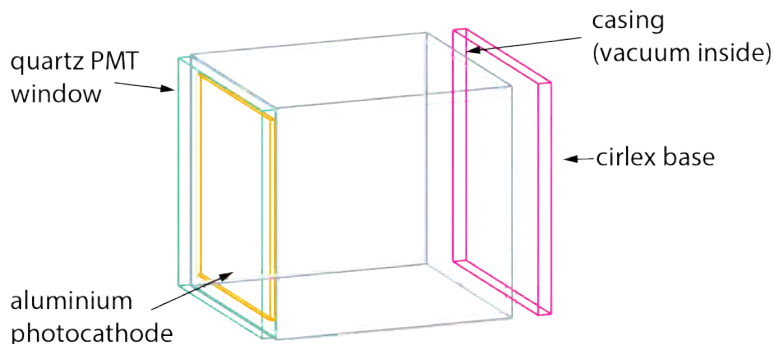


Figure 3.2: Overview of one simulated bottom photomultiplier tube.

Some detector properties are designed to be changeable during two runs of the simulation process. These properties are preset in the detector construction with a recommended value so that the simulation can be used without knowing how to adjust all parameters. The absorption length of liquid xenon, the reflectivity of PTFE, the material of the meshes in liquid or gaseous xenon and the material of the liquid xenon volume are changeable. This makes it possible to simulate also e.g. a single phase xenon time projection chamber.

All in all, the simulation is not only including the detector geometry (see figure 3.3), but it also implements all possible physical processes and interactions which may happen in each volume. With this feature any possible change of the detector geometry and its influence onto the system can be studied and analyzed.

¹In the Muenster TPC experiment used PMTs (R8520-06SEL) have a photocathode consisting of bialkali. The properties of this material are transferred to the used aluminium photocathodes within the simulation.

In the scope of this thesis the simulation package is ready for studies on the detector response for scintillation light, variation of different parameters of the main volumes and gamma calibrations with different radioactive sources.

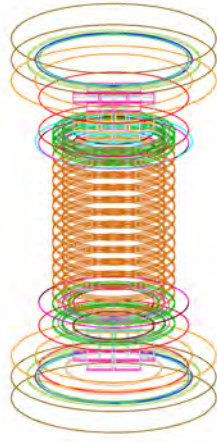


Figure 3.3: Setup of the different volumes in the simulation. Only the outer edges of each volumes are drawn. The insulating vacuum chamber is neglected.

Further information regarding the simulation package can be found in the source code and documentation. The functionality of the simulated detector can be observed by checking the track of a particle through the detection volumes.

3.1.2 Particle tracking and basic detector response

After implementing the geometry for the first time and on every change in the volume dimensions, GEANT4 offers the possibility to check the placement of every volume by sending non interacting particles through the detector. These particles, called *geantino*, are placed in the laboratory outside of the detector with a certain direction through the volumes. By doing so, the boundaries between all volumes can be checked. For this, particle track information, in which all passed volumes, positions, energies and particle types are listed, can be analyzed. This check was done for different directions and positions. The detailed track information should be used for testing purposes only and slow down the simulation process.

The particle interactions in GEANT4 can be divided in two categories: The propagation of xenon scintillation light and the interaction of particles in the detector volumes. In the first case, the GEANT4 toolkit uses *optical photons* that follow geometric optics, including reflection and refraction and can scatter via Rayleigh scattering or be absorbed in the xenon. For liquid xenon, the absorption length is varied to model different electronegative impurity levels with a predefined value of 20 cm, and the Rayleigh scattering length is set to 30 cm.

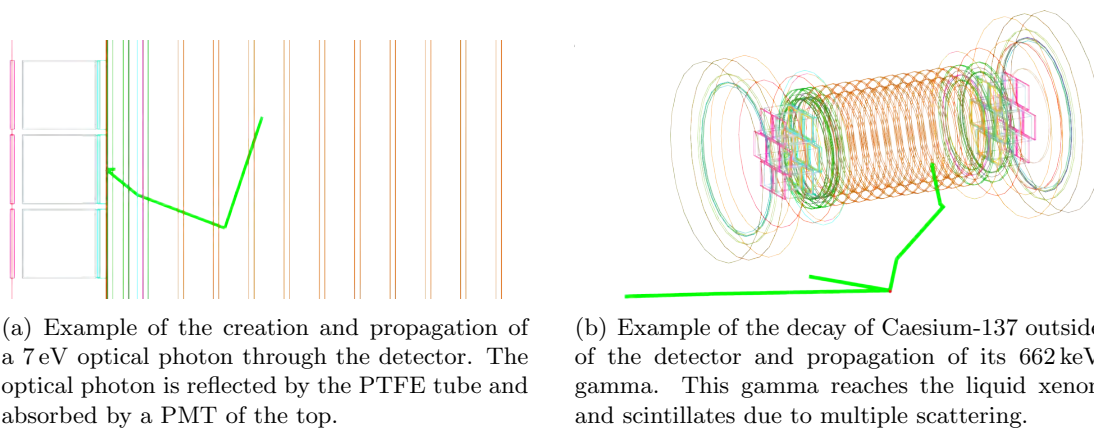


Figure 3.4: Visualization of the Particle Tracking in GEANT4 with the QT visualization driver. The TPC is drawn rotated so that the top is on the left side. Green lines indicate the tracks of photons, while red lines would visualize the track of electrons. The scintillation light is not visible in the visualization of gamma simulations.

All previously described interactions (see section 2.2.2) are possible for the interaction of particles. GEANT4 uses tabulated cross sections to model all possible interactions correctly.

In order to clarify the working principle of the simulation package, two basic examples with one simulated event, or primary particle, are shown in figure 3.4. The simulation of optical photons, seen in figure 3.4(a) is realized by creating one single 7 eV optical photon randomly inside the liquid xenon. The photon propagates to the PTFE tube wall and is reflected to the surface of the liquid xenon, which is indicated by a light blue line. The photon is refracted on the liquid xenon surface and then absorbed by a top PMT. This kind of simulation will be discussed in section 3.2 of the following chapter. A typical event of a gamma simulation, in this case ^{137}Cs , is visualized in figure 3.4(b). The gamma source is placed outside of the Muenster TPC and decays to ^{137}Ba while emitting a 662 keV gamma (see section 3.3). This gamma is refracted at the cryostat and gives a scintillation signal after a scattering process. In this type of simulation, the tracking of scintillation light is disabled.

In the Muenster TPC simulation the particle type, direction, energy and position of the source can be defined by the *ParticleSourceMessenger* without the need to recompile the whole simulation package. If the particle type *ion* is used, it can be built by defining the atomic number, atomic mass, charge and excitation energy.

3.2 Scintillation light propagation

As introduced before, simulations of the Muenster time projection chamber are necessary to understand its light response. The simulations for analyzing the scintillation light propagation are realized by generating isotropic 7 eV photons (178 nm) uniformly throughout the detection volume. Using this method, the LCE can be determined by the fraction of light that hits a PMT and the total amount of light inside the TPC. Therefore, it is enough to obtain the number of PMT hits and the amount of generated photons for a specific detector region.

In order to prove that the rebuild of the Muenster TPC simulation is working properly, the LCE will be compared to the previous results [8] and figure 2.2 [7]. In addition to this, the impact of the absorption length of xenon and reflectivity of PTFE on the LCE or LY will be shown, as well as simulations on one-phase TPC setups.

3.2.1 Light collection efficiency

As described in section 2.2, the LCE depends on various geometrical and physical effects. Because the Muenster TPC and the XENON100 detector are comparable, a similar behavior of the LCE can be expected. Both detectors are axially symmetric, but the Muenster TPC has a more cylindrical shape. Therefore, the LCE should not decrease while increasing the radius as seen for XENON100 in figure 2.2. Due to the possible reflection at the transmission of the liquid xenon to the gaseous, the LCE at the bottom of the TPC should be much higher than at the top.

In order to extract the LCE out of the simulation data for each tracked particle an additional program for analysis is developed, which divides the TPC in volumes and evaluates the LCE as the fraction of PMT hits to the number of totally generated photons created in each volume. For obtaining the LCE of the Muenster TPC 10^8 optical photons with an energy of 7 eV are simulated. These optical photons are uniformly distributed and confined to the liquid xenon volume. The liquid xenon absorption length is set to 20 cm and the reflectivity of PTFE is implemented as 95%. In addition to this another geometrical effect has to be considered.

Because grids can not be directly implemented in GEANT4, the grid meshes in the simulation are added as a solid volume with properties of a grid. This means, that the meshes have a refractive index which controls the permeability. This induces different refractive indices for meshes surrounded by different volumes. If this is not considered and no suitable refractive index is used, the photons will not pass the mesh anymore. The prior simulation package used a refractive index, which is the same as for gaseous xenon, for all meshes, also for these

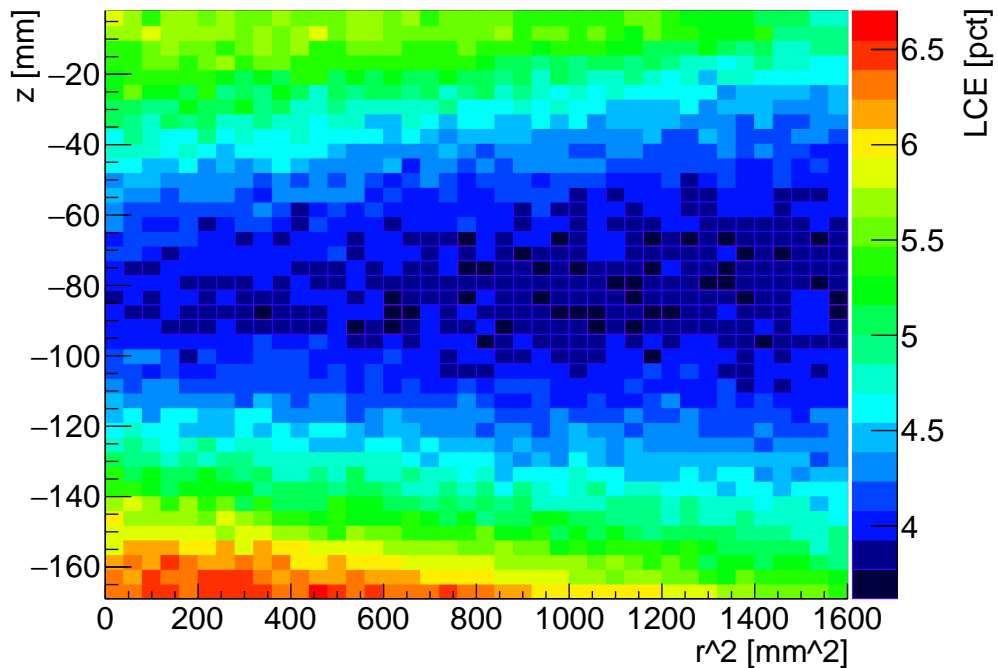


Figure 3.5: Light collection efficiency map for 7 eV optical photons confined by the liquid xenon volume of the two phase Muenster TPC, assuming all meshes have the gaseous xenon refractive index of 1. The LCE to the total amount of generated photons is given by the color. The simulation is done with a liquid xenon absorption length of 20 cm and a PTFE reflectivity of 95% for 10^8 uniformly distributed optical photons or events.

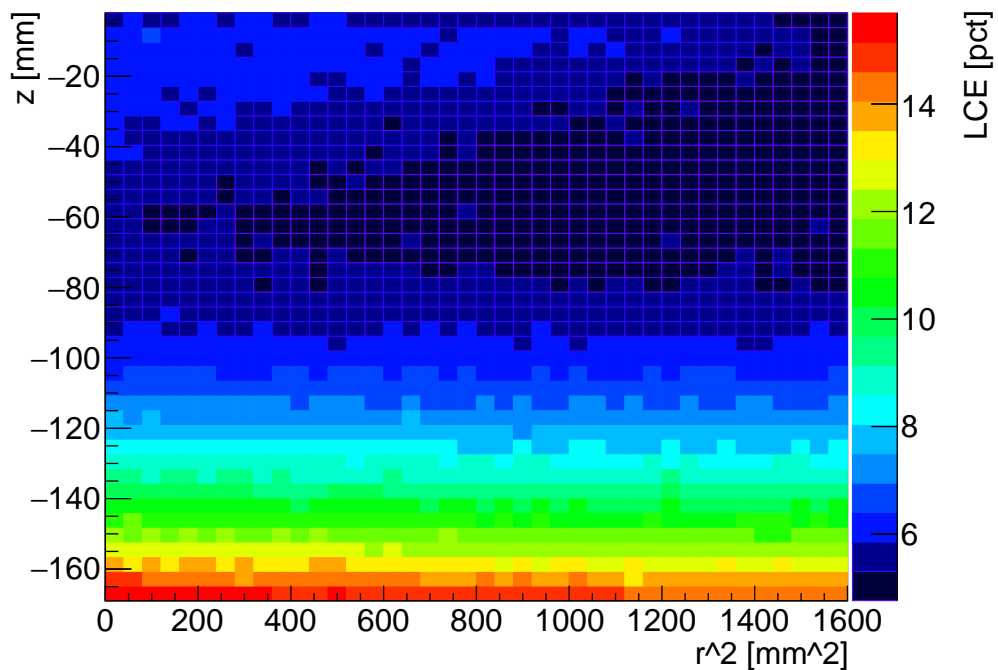


Figure 3.6: Light collection efficiency map for 7 eV optical photons confined by the liquid xenon volume of the two phase Muenster TPC, assuming each mesh have the refractive index defined by its outer volumes, which is 1.3 for meshes in liquid xenon and 1 for meshes in gaseous xenon. The LCE to the total amount of generated photons is given by the color. The simulation is done with a liquid xenon absorption length of 20 cm and a PTFE reflectivity of 95% for 10^8 uniformly distributed optical photons or events.

in the liquid phase. This leads to huge influence of the LCE as the photons are refracted and distracted at the cathode (figure 2.1). Thus, more photons are absorbed by the liquid xenon. Therefore the refractive indices of the meshes are designed to be changeable in the updated simulation package. According to this, the LCE simulations are done twice for different setups of the meshes. The first setup matches the simulation setup in [8], while the second setup defines the refractive index of the meshes by its outer volumes.

The LCE of the Muenster TPC simulation as a function of the vertical position z and the radius squared r^2 is shown in figure 3.5 and 3.6. As expected, the LCE is much higher at the bottom of the TPC and decreases with increasing radius. The LCE map seen in figure 3.5 has two areas with higher values of the LCE at the top and the bottom of the TPC. However the top area has an equal value as in figure 3.6, but due to different refraction indices photons are refracted at the cathode and thus have a longer path. Therefore these photons are more often absorbed by the xenon. Thus, the LCE in the detector is reduced. The LCE shown in figure 3.6 is not as large on the top as on the bottom of the TPC, due to the reflection at the surface of the liquid xenon. The decrease of the LCE with increasing radius can be confirmed by the consideration that for photons starting in the center of the TPC the range of possible momentum angles, which is directly connected to the detection of the photons, in case it is not scattered, is larger than for photons starting in outer regions of the TPC. This behavior was also seen in [8]. Therefore, the average LCE can be obtained as $\text{LCE} = \frac{N_{det}}{N} = 4.59\%$, in which N_{det} is the number of detected photons by any PMT, after simulating N photons in the liquid xenon volume, neglecting the quantum efficiency.

The behavior of the LCE map for sufficient refraction indices of the meshes, which makes the meshes transparent for photons, can be seen in figure 3.6. Again the LCE map shows the expected behavior, except the less distinct top area, meaning the gate mesh has the same refraction index as the liquid xenon around it and photons are no longer refracted. However the top area still has a radius dependent behavior. Due to this, the average LCE is $\text{LCE} = 7.24\%$. This LCE map also shows the in section 2.2 elucidated behavior of the XENON100 LCE map (figure 2.2), which can be compared due to the similar detector geometry. Both exhibit a decreasing progression of the LCE with increasing z . To fully compare both findings, the LCE map seen in figure 3.6 is converted into a relative LCE map by the use of the average LCE value, as seen in figure 3.8.

The relative LCE seen in figure 3.9 with an assigned absorption length for liquid xenon of 100 cm, which is chosen due to the assumed value of 100 cm in the XENON100 experiment, shows the same behavior as the relative LCE map for the XENON100 TPC [4]. Note that the relative LCE seen in figure 3.7 displays a different behavior, as described before. This is an additional cross check that the detector works as expected if the meshes have the same

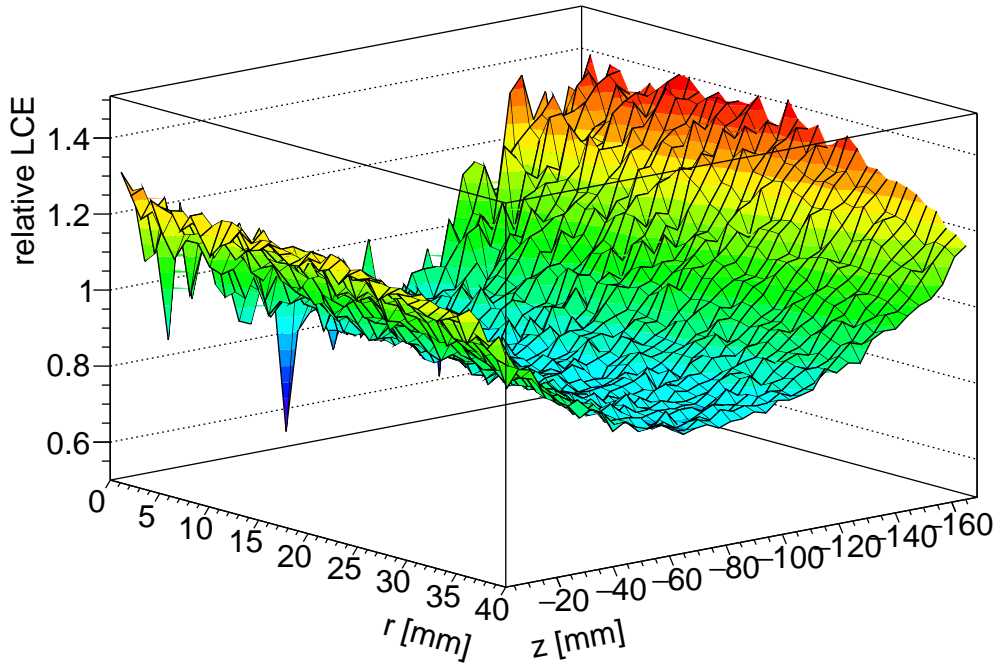


Figure 3.7: Relative light collection efficiency map for 7 eV optical photons confined by the liquid xenon volume for the Muenster TPC, assuming all meshes have the gaseous xenon refractive index. The light collection efficiency is plotted relatively to the average LCE for a liquid xenon absorption length of 20 cm, a PTFE reflectivity of 95 % and 10^8 events.

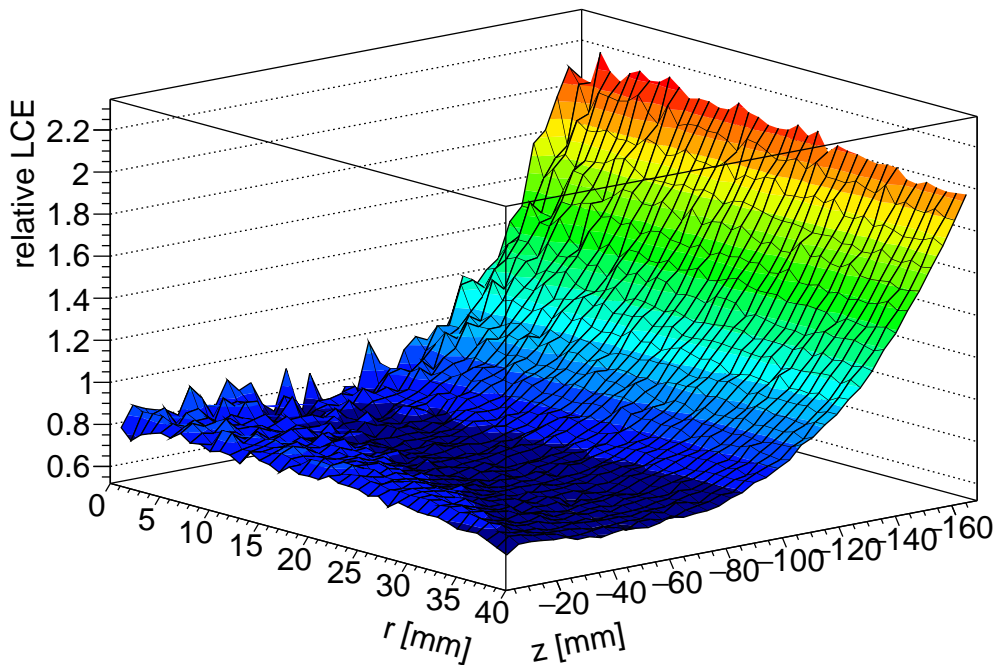


Figure 3.8: Relative light collection efficiency map for 7 eV optical photons confined by the liquid xenon volume for the Muenster TPC. The light collection efficiency is plotted relatively to the average LCE for a liquid xenon absorption length of 20 cm, a PTFE reflectivity of 95 % and 10^8 events.

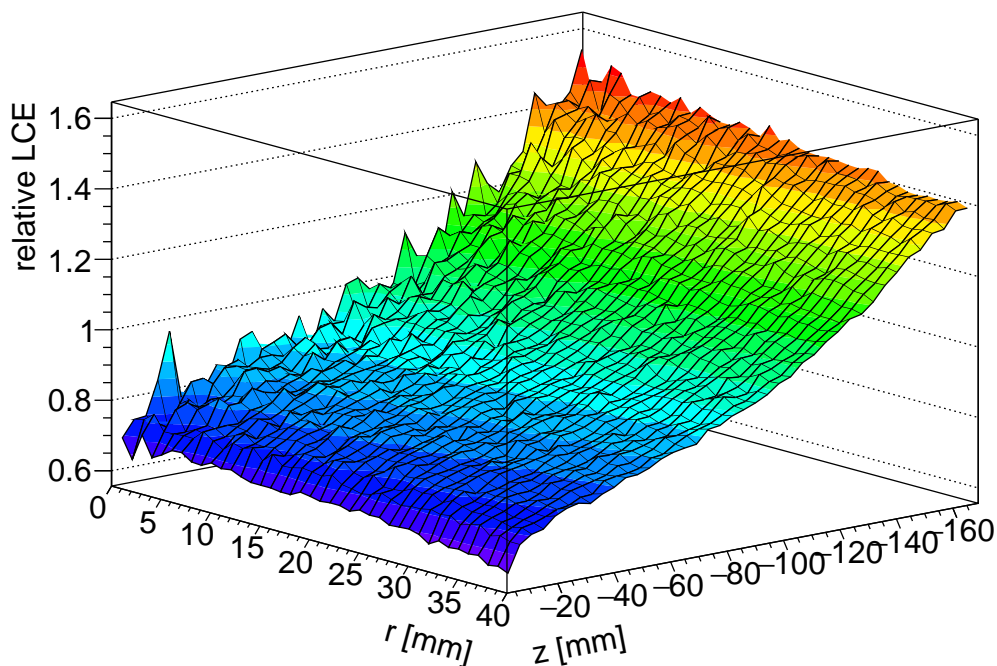


Figure 3.9: Relative light collection efficiency map for 7 eV optical photons confined by the liquid xenon volume for the Muenster TPC. The light collection efficiency is plotted relatively to the average LCE for a liquid xenon absorption length of 100 cm, a PTFE reflectivity of 95 % and 10^8 events.

refractive index as their surroundings. Therefore, only this detector setup is considered in the following.

However, if needed the detector material was designed to be changeable in the simulation setup. Because of this, it is also possible to perform simulations for a single phase TPC filled with gaseous xenon. For this, the meshes are also defined with the refraction index of gaseous xenon.

Using this for a single-phase (gaseous) xenon TPC, the average LCE value for the LCE map seen in figure 3.10 can be obtained as $LCE = 30.49\%$. This average LCE is much higher than for the dual phase xenon TPC, which is a result of the missing of the liquid xenon surface. Therefore, a sufficient implementation of parameters such as the absorption length of xenon or the reflectivity of PTFE is essential. These impacts will be studied in the following chapter, as well as 3D light yield maps to detect small scale variations in different detector regions.

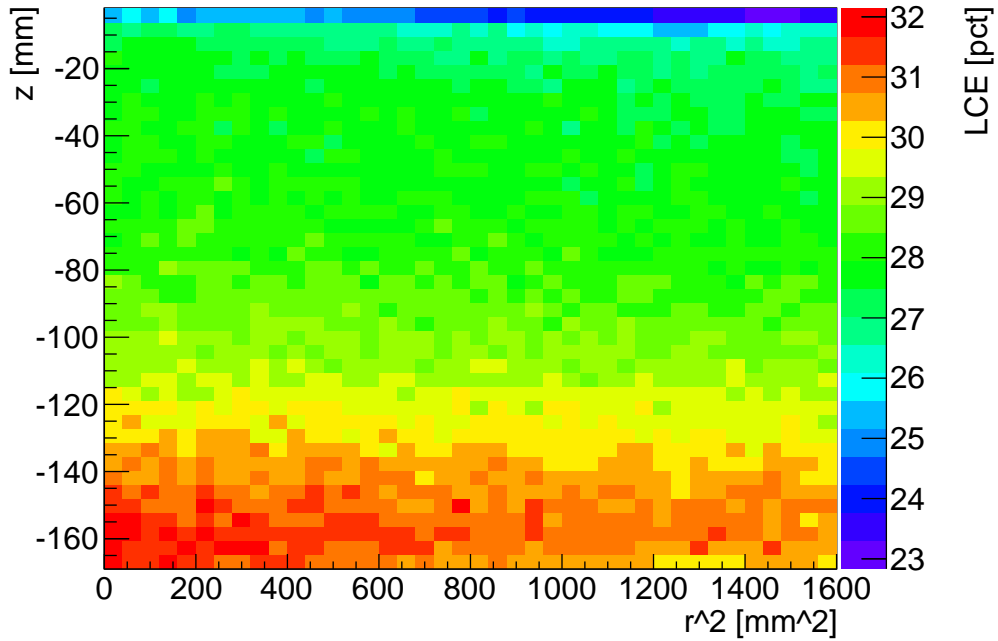


Figure 3.10: Light collection efficiency map for 7 eV optical photons confined by the gaseous xenon volume in a full gaseous xenon time projection chamber with sufficient meshes, which have the same refraction index as gaseous xenon. The simulation is processed with 10^8 initial events, a liquid xenon absorption length of 20 cm and a PTFE reflectivity of 95 %.

3.2.2 Light yield

As mentioned in section 2.2, the TPC can also be described by a light yield. In order to perform this light yield calculation in a three-dimensional way, which offers the possibility to do a check of the small scale symmetry of different detector volumes, the detector is divided into 1000 volumes, 10 volumes in each direction. The light yield in each of these volumes can be obtained by the following equation²:

$$LY_i = \frac{1}{W} \cdot \frac{QE \cdot N_i}{N_{\text{initial}}} \quad (3.1)$$

In this light yield calculation, W is the average energy that is required to produce one scintillation photon as explained in section 2.1, QE is the average quantum efficiency of the PMTs, N_i is the number of photons that hits the PMTs, generated in each volume, and N_{initial} is the simulated number of photons in each volume. Due to the uniform distribution of the optical photons, N_{initial} can also be obtained as $N_{\text{initial}} = N_{\text{simulated}} \cdot \frac{V_i}{V_{\text{tot}}}$, in which $N_{\text{simulated}}$ is

²Other physical effects, such as the relative scintillation efficiency, are neglected.

²Only this W value is considered in the simulations even though the LY is energy dependent.

the total amount of simulated photons, V_i the fraction of the volume and V_{tot} the volume of the whole TPC. The resulting map is shown in figure 3.11.

Four certain z regions are shown in figure 3.11, from the top, the upper middle, the middle and the bottom. As seen before, the LY is much higher at the bottom ($z = -152.30$ mm to $z = -169$ mm), with values of (2.1 ± 0.1) pe/keV in the z region of 16.7 mm height, as at the top ($z = -2$ mm to $z = -18.70$ mm), with values of (0.9 ± 0.1) pe/keV. As expected before, the LY decreases for higher radii, but no asymmetry or variation in the detector geometry can be obtained. This is also a check to see if the simulation package is working properly. This LY value is highly depending on geometry properties such as the absorption length of liquid xenon or reflectivity of PTFE. Therefore, further simulations with different geometry properties are done.

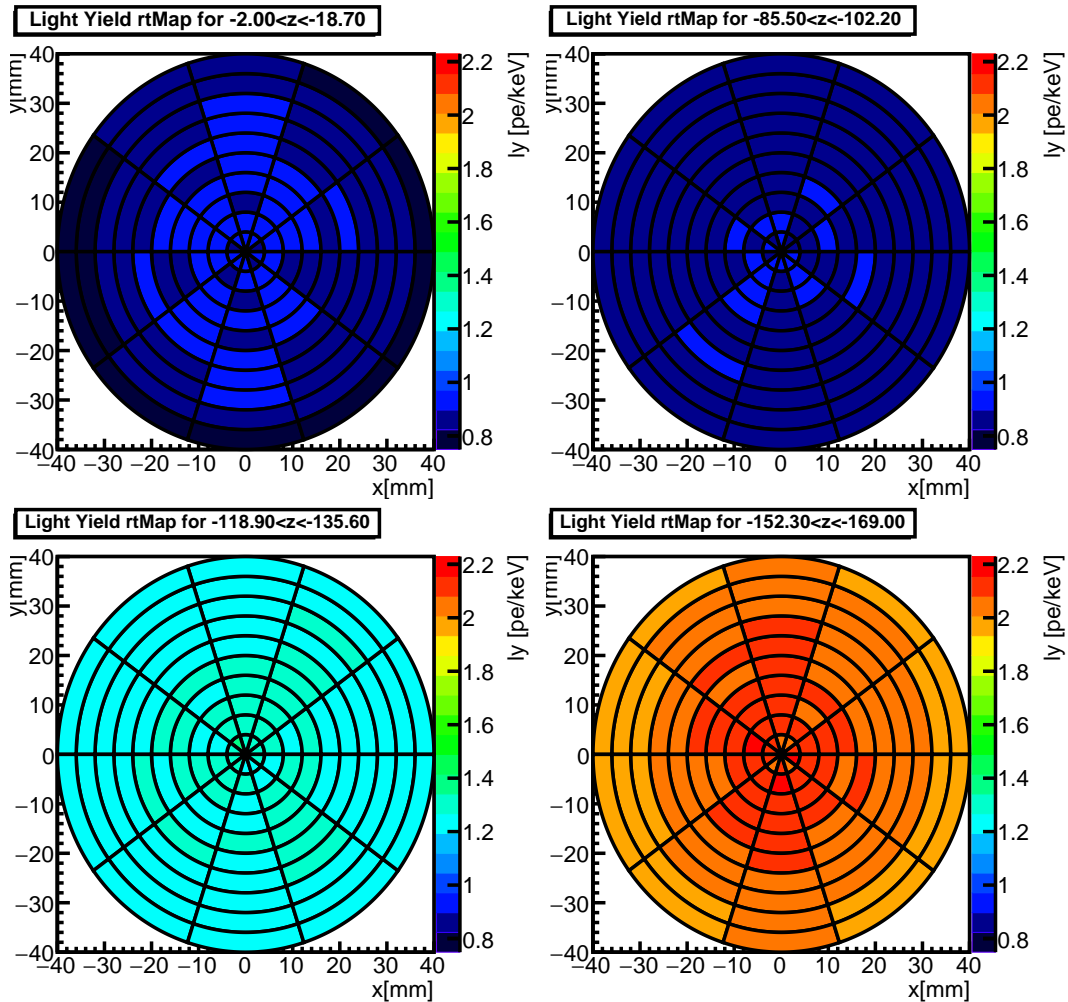


Figure 3.11: Light yield maps for different volumes in z direction of the Muenster TPC. All meshes are sufficiently implemented with a refraction index defined by the volumes around. The simulation is processed with 10^8 events, a PTFE reflectivity of 95 % and an attenuation length of 20 cm for liquid xenon.

Influence of the absorption length

The influence of the liquid xenon absorption length on the LY can also be investigated as the impact of the xenon purity on the LY because the absorption length varies as a function of xenon purity. The absorption length describes the propagation length of photons without interactions in the propagation volume. As a result of this investigation, the optimal purity of xenon, which should be used to reach the maximum LY, can be determined.

In order to obtain this function, different simulations with different absorption lengths are done, and the average LY in the detector against the absorption length is plotted in figure 3.12.

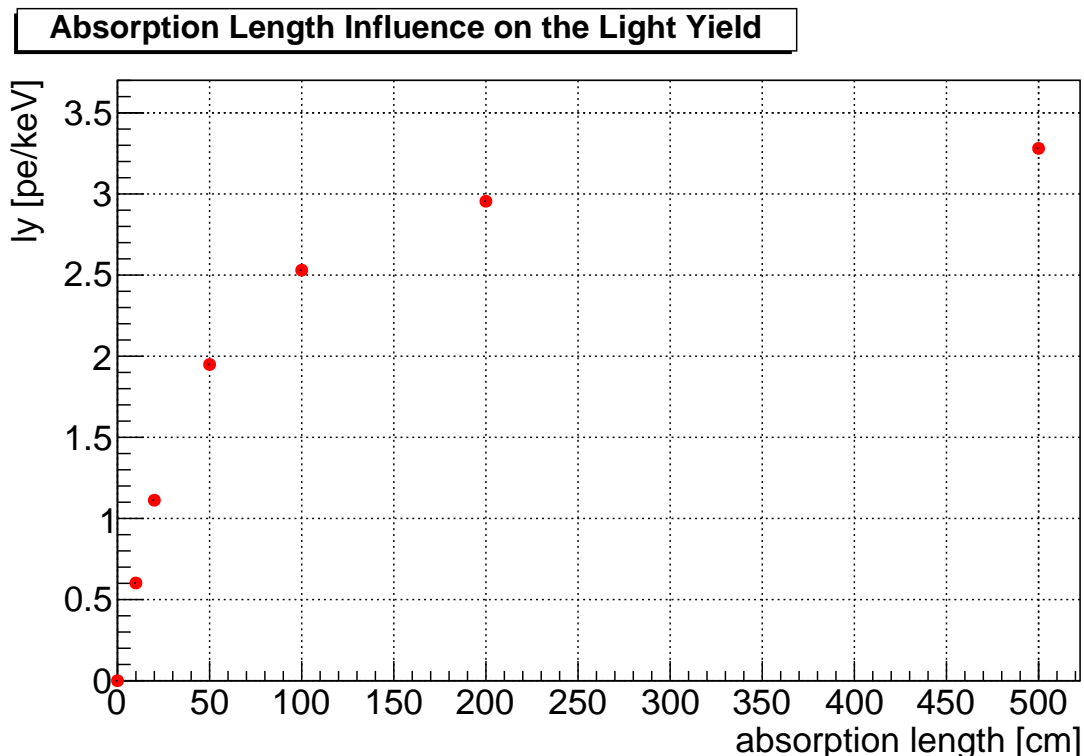


Figure 3.12: Influence of the absorption length on the light yield for 7 eV optical photons confined by the liquid xenon volume, simulated with a PTFE reflectivity of 95 %.

According to this, the LY is strongly dependent on the absorption length for small scales up to 200 mm. However, the defined size of the TPC makes the system less sensitive for higher absorption lengths, since the absorption length exceeds the dimensions of the Muenster TPC by more than an order of magnitude, which means that almost all photons will be detected. The LY can be increased not only by improving the purity of xenon, but also by optimizing the reflectivity of PTFE.

Influence of the reflectivity

The impact of the PTFE reflectivity can be obtained by simulating the LY map for different values of the reflectivity. Therefore, different reflectivity values are implemented for the PTFE and can also be changed without the need of recompiling the simulation package.

This study must also be done to determine the reflectivity of PTFE for the Muenster TPC experiment. In order to obtain this, the measured LY can be matched with the simulations, shown in figure 3.13.

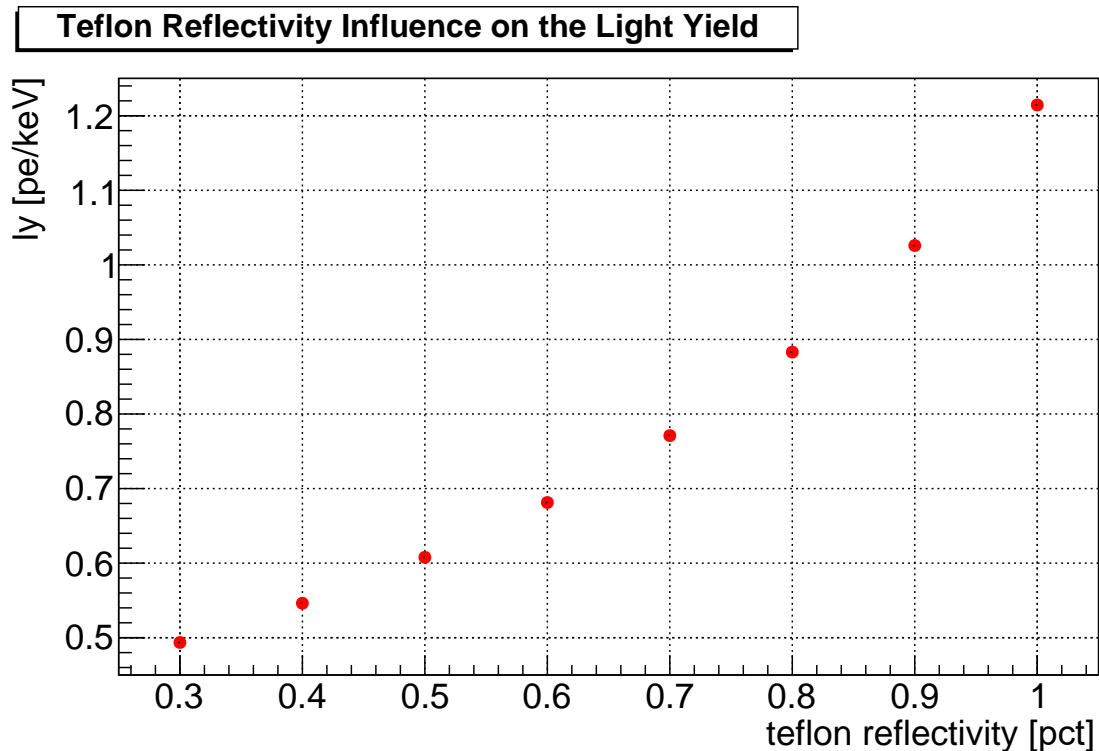


Figure 3.13: Influence of the Teflon reflectivity on the light yield for 7 eV optical photons confined by the liquid xenon volume, simulated with an absorption length of 20 cm.

As it can be seen in figure 3.13, the LY increases with a higher reflectivity value. To obtain the LY in the Muenster TPC experiment, various calibration sources can be used.

3.3 Calibration simulations of the Muenster time projection chamber

Calibrations for liquid xenon detectors and especially for the Muenster TPC can be realized with gamma sources. Due to the large amount of possible sources, calibration simulations are necessary to choose the appropriate one, which can be easily used to determine the LCE and LY. In the following, three possible gamma sources, ^{57}Co , ^{60}Co and ^{137}Cs , will be presented and tested. The simulations are performed with the same number of initial events and with the same primary position outside of the TPC (see figure 3.14), which could be varied for the Muenster TPC experiment. This ensures a comparable behavior of each source and makes it possible to draw a clear conclusion about the choice of a sufficient source. An optimal source for calibration purposes would reach the entire detection volume, the liquid xenon, uniformly and thus give scintillation signals out of all possible positions. However not only the coverage of the whole detection volume, but also the calibration in a certain range of energy should be considered. Especially the PTFE is chosen to get a high reflectivity for xenon photons. Therefore the reflectivity for photons of a various energy could be different. In order to also consider this photon energy dependence, the low energy radioactive source

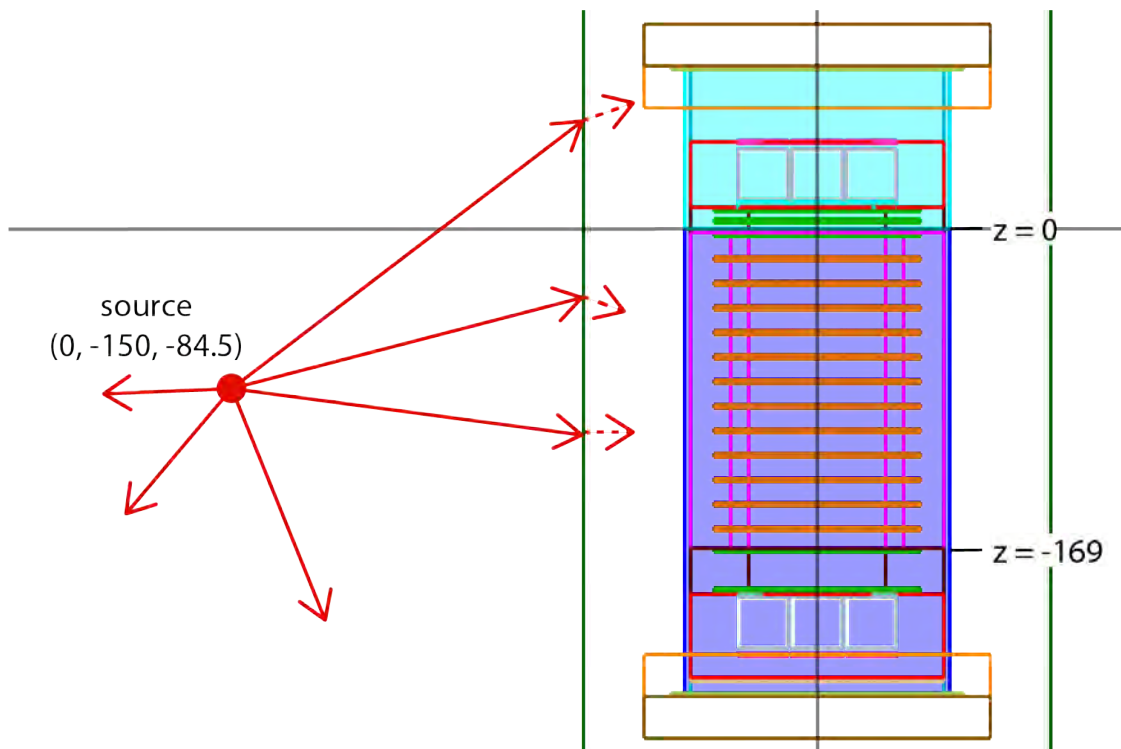


Figure 3.14: Sketch of the center-left source position (red circle) for the gamma simulations of the Muenster TPC. The red arrows show possible photon propagations until they reach the insulating vacuum chamber.

^{83m}Kr , which excites the xenon via beta decay and thus producing xenon scintillation light, will be considered in the following as well.

The results of the different simulations are checked by verifying the decay processes and occurred particle types as well as the track positions of the particles. The taken data is stored in *root* files and can be used to reconstruct every important step of the simulations afterwards.

3.3.1 ^{57}Co

The first simulated and tested gamma source with a half-life of 271.74 d is ^{57}Co , which is widely used for medical purposes [6]. ^{57}Co mainly decays by emitting a 122.1 keV and 136.5 keV gamma. It is implemented to GEANT4 as an *ion* source presented in the decay scheme shown in figure 3.15.

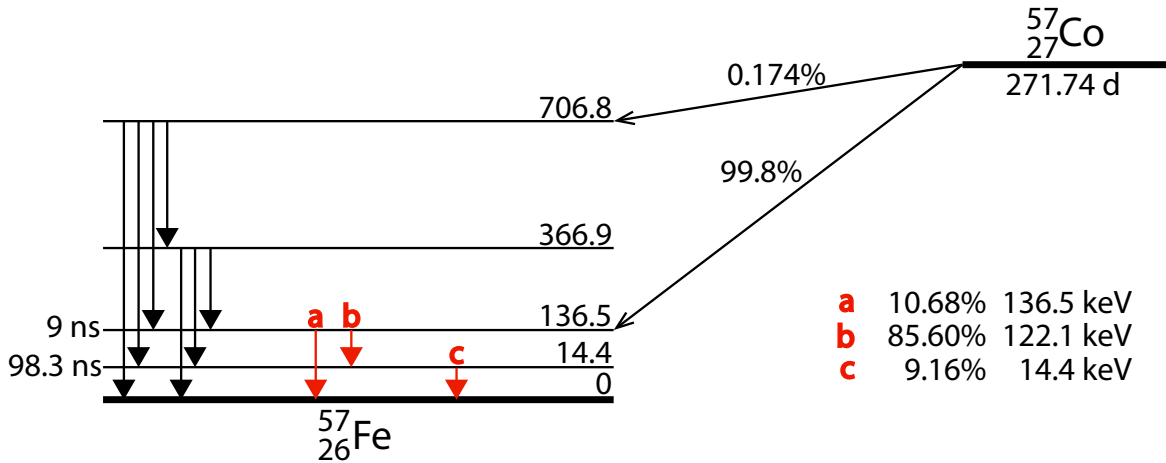


Figure 3.15: Decay scheme of ^{57}Co (with the use of [2]).

In order to test the calibration quality of this source, a simulation with 10^7 events is taken, which means that 10^7 ^{57}Co particles are simulated with no excitation energy at a certain position. Therefore, the ^{57}Co is placed outside of the TPC at position $(0, -150, 84.5)$, which can be obtained in figure 3.14 as center-left of the liquid xenon volume, where $(0, 0, 0)$ is set to the center of the liquid xenon surface. As outlined before, the decay process will be performed by GEANT4 with the assistance of decay tables. Because the scintillation light is less important for this simulation, it will not be simulated. The energy spectrum can be directly extracted out of the deposited energy in the detection volume of the TPC simulation, which is stored in the simulation data for each event or ^{57}Co particle, and is presented in figure 3.16.

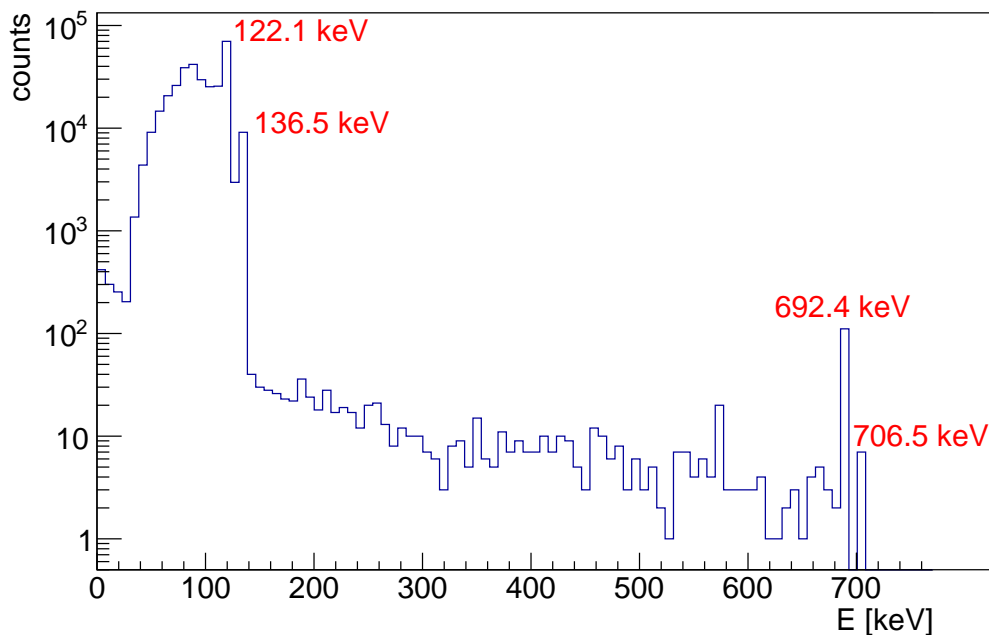


Figure 3.16: Simulated spectrum of ^{57}Co , placed outside the TPC at position $(0, -150, 84.5)$, taken out of the deposited energy of 10^7 initial ^{57}Co particles.

As expected from figure 3.15, the 122.1 keV and 136.5 keV peaks of ^{57}Co are clearly visible in the spectrum shown in figure 3.16. The broader parts of this spectrum below these peaks occur due to single and multiple Compton scattering in the stainless steel and PTFE, as described in section 2.2.2. Therefore, the gammas have a lower energy when they are absorbed in the xenon volume. This effect can be observed for all gamma sources which have to be positioned outside the TPC.

In order to make a statement about the quality of this calibration source, the positions of events in the liquid xenon are mapped out. With this map, seen in figure 3.17, the penetration depth and angular distribution of the gammas can be determined. The event map of the detection volume is divided into 1600 volumes and covers the z range from -2 to -169 , which does exclude the gate mesh. On the z axis, the percentage of the events which took place in a certain volume of the total sum of all events, which is 478638 events, is given. An ideal calibration source can pass through the whole detector and trigger events in each part of the detection volume. This can also be achieved by placing the sources at different positions around the TPC if they reach at least the middle of the detection volume.

As can be observed in figure 3.17, ^{57}Co only reaches the first 10 mm of the liquid xenon. However this was expected from the decay energy of it. The gammas have a mean free path of 0.07 cm in liquid xenon, which is not enough to reach the middle [8]. This discards the use of ^{57}Co for calibration purposes.

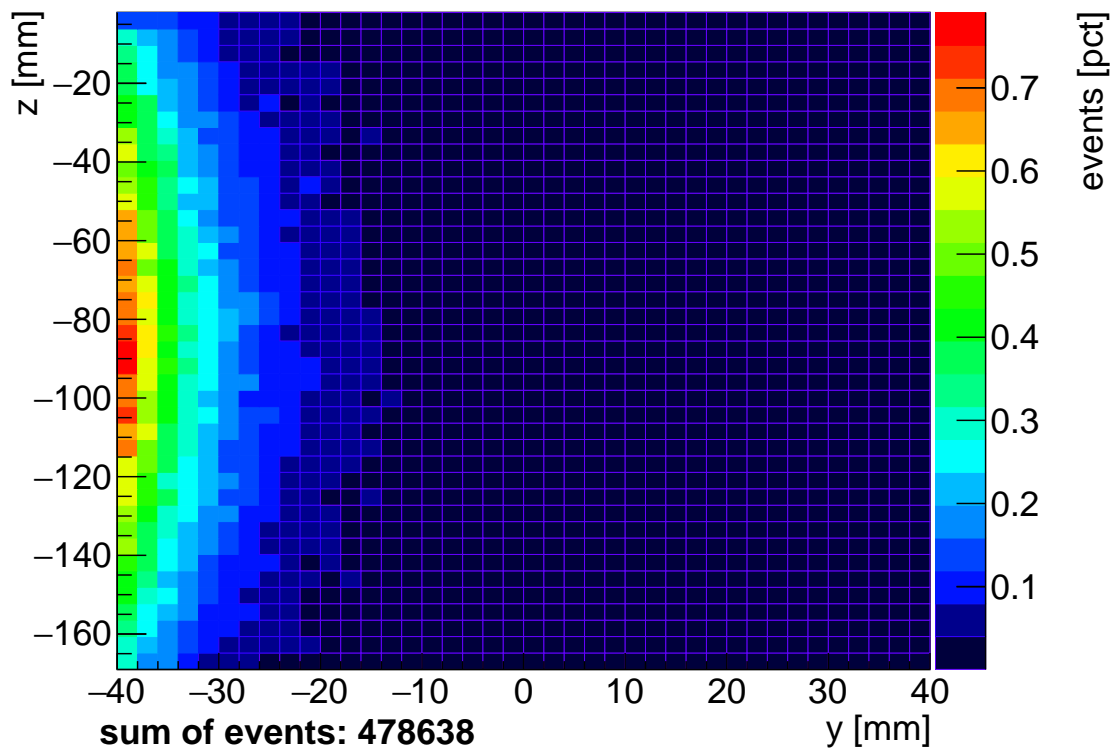


Figure 3.17: Position of events or interactions in the Muenster TPC for ^{57}Co , placed outside the TPC at position $(0, -150, 84.5)$. The simulation is processed with 10^7 ^{57}Co events, a liquid xenon absorption length of 20 cm and a PTFE reflectivity of 95 %.

In order to reach the middle of the Muenster TPC, a source with an improved mean free path of about 40 mm has to be taken. This criterion is fulfilled either by ^{60}Co or ^{137}Cs .

3.3.2 ^{60}Co

In order to improve to a penetration of the middle of the detection volume, ^{60}Co with a half-life of 1925.28 d is chosen. ^{60}Co has a mean free path of 50 mm and mainly emits 1.17 MeV and 1.33 MeV gammas, therefore ^{60}Co should reach the middle of the liquid xenon. The decay scheme of it is shown in figure 3.18.

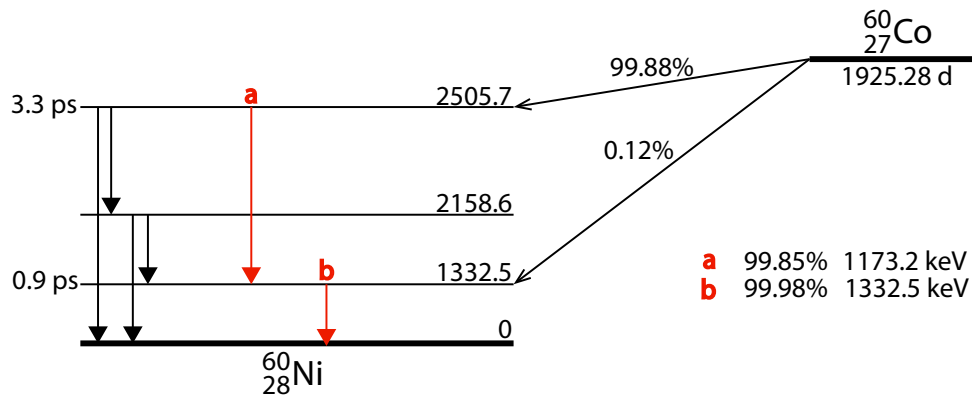


Figure 3.18: Decay scheme of ^{60}Co (with the use of [2]).

Again the simulation is performed for 10^7 events or ^{60}Co particles, which are placed as before, on the left-middle of the TPC. ^{60}Co is implemented in the same way as ^{57}Co was

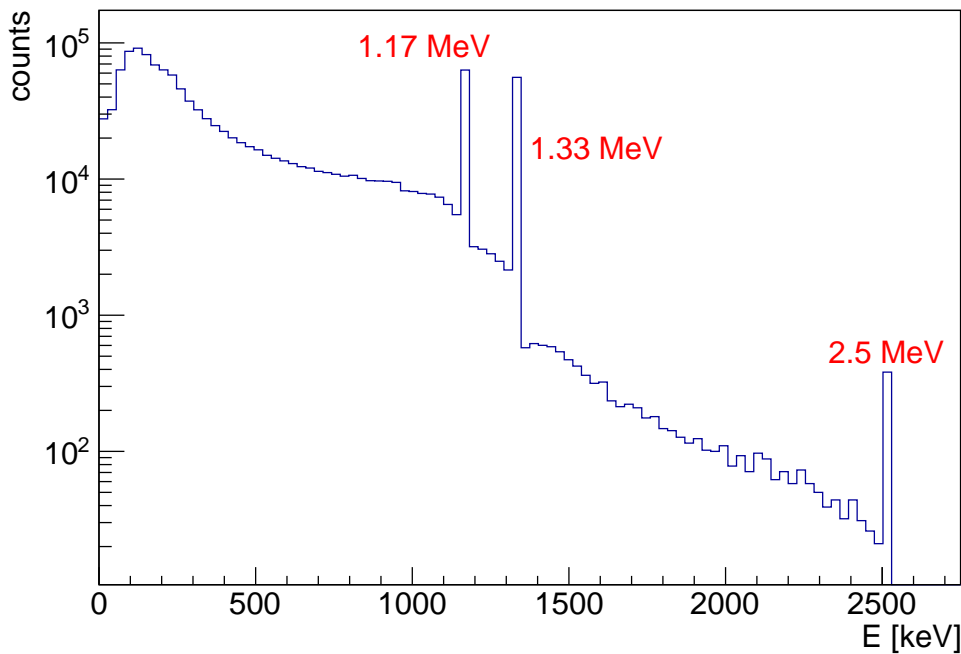


Figure 3.19: Simulated spectrum of ^{60}Co , placed outside the TPC at position $(0, -150, 84.5)$, taken out of the deposited energy. The small peak at 2.5 MeV can be obtained as the sum line from the two high probability peaks 1.17 MeV and 1.33 MeV.

before. The simulated energy spectrum can directly be obtained from the data and is presented in figure 3.19.

The two high probability peaks, 1.17 MeV and 1.33 MeV, are clearly visible. A small peak, which is the sum line from the two high probability peaks, can also be seen at 2.5 MeV. As mentioned before, a lot of backscatters and Compton scatters are also shown, which occur due to interactions with the stainless steel or PTFE. Therefore, the spectrum of ^{60}Co satisfies the expectations and verifies the simulation processing. After this an event map of the TPC profile is determined in the same way as before. This ensures a comparable presentation in which the total amount of events has to be considered.

As can be observed in figure 3.20, the ^{60}Co source reaches the center of the liquid xenon with a percentage of about 0.08. The most events take place in z range from -135 mm up to -50 mm and radius from -40 mm up to -15 mm, in which the highest value is 0.12% of the total amount of events. Additionally, there are also events on the whole z range of the liquid xenon, which is an important feature of the source. Due to this, ^{60}Co needs only to be placed around the TPC and not to be shifted on different z positions, in order to reach the whole

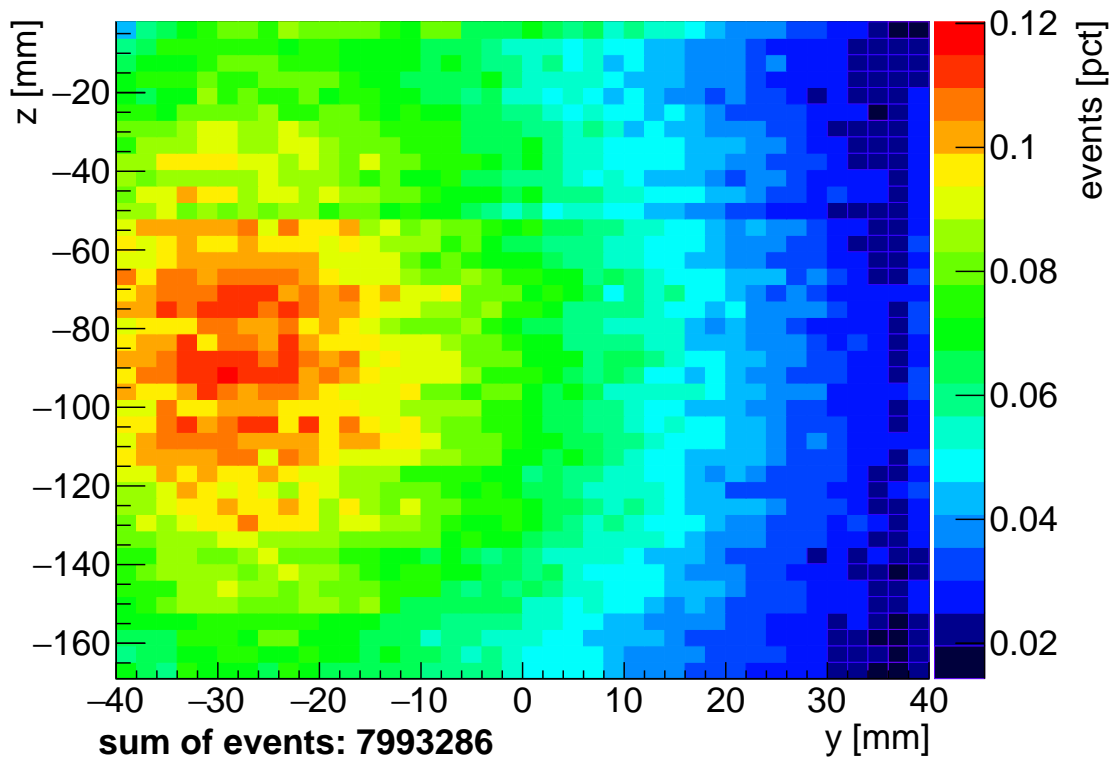
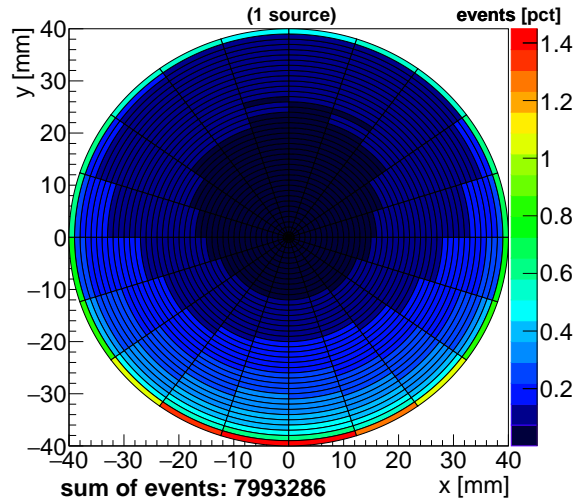


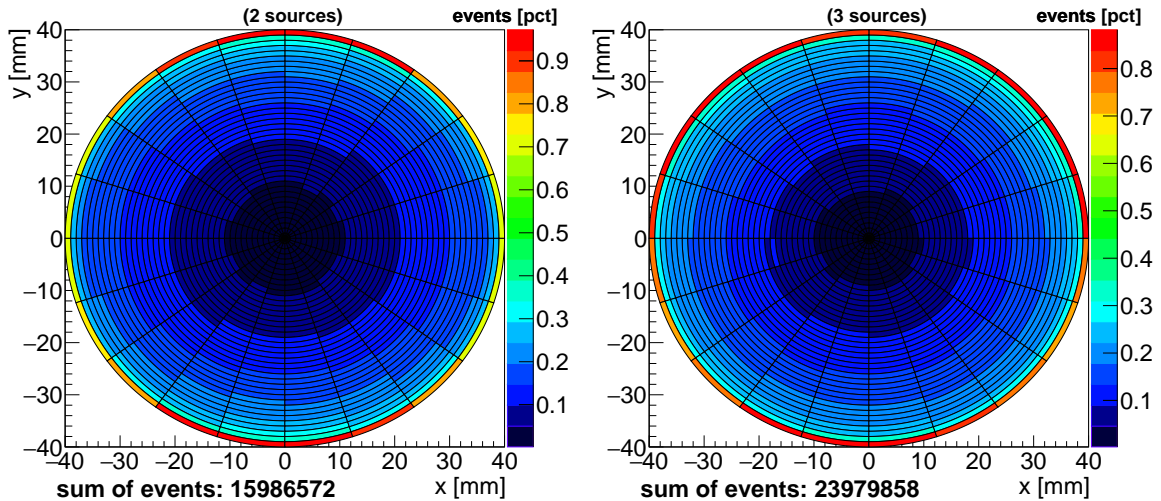
Figure 3.20: Position of events or interactions in the Muenster TPC for ^{60}Co , placed outside the TPC at position $(0, -150, 84.5)$. The simulation is processed with 10^7 ^{60}Co events, a liquid xenon absorption length of 20 cm and a PTFE reflectivity of 95 %.

detection volume. The needed amount of circular positions can be obtained by mapping out the events in a xy -plane and simulate several equal sources at different positions in once.



(a) Position of events or interactions in the muenster time projection chamber.

Figure 3.21: Results of the simulations for ^{60}Co placed outside the time projection chamber at position $(0, -150, 84.5)$. The simulation is processed with 10^7 ^{60}Co events, a liquid xenon absorption length of 20 cm and a PTFE reflectivity of 95 %.



(a) Results of the simulation of two sources placed opposite to each other. (b) Results of the simulation of three sources uniformly placed around the TPC.

Figure 3.22: ^{60}Co simulations with different amount of sources. The simulations are processed with 10^7 ^{60}Co events, a liquid xenon absorption length of 20 cm and a PTFE reflectivity of 95 %.

The circular event map for ^{60}Co is shown in figure 3.21 and exhibits an decreasing amount of events while approaching the middle of the TPC, as well as lower amount of events in the opposite side of it. The shape of this event distribution is neither uniform nor symmetrical. Therefore, placing the source at different positions is necessary. In order to prove this two basic simulations with two and three sources or source positions are implemented, processed and superpositioned (figure 3.22). According to these simulations, it can be determined that at least three positions of the ^{60}Co source are required to get a symmetrical event mapping, which corresponds to a uniform distribution.

In summary, ^{60}Co can be used to do gamma calibrations of the Muenster TPC for energies of 1.17 MeV and 1.33 MeV. During the calibration process it only has to be moved on at least three positions around the TPC. This calibration process will take 10 s each position, since a 1 MBq ^{60}Co source and 10^7 required events are assumed.

3.3.3 ^{137}Cs

As can be seen in the decay chain pictured in figure 3.23, ^{137}Cs has 662 keV decay with a mean free path in liquid xenon of 40 mm and a half-life of 30.08 y.

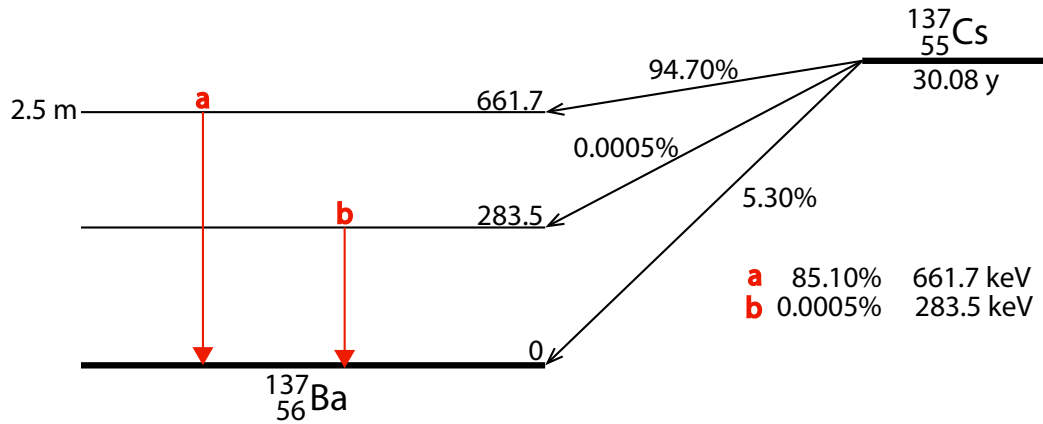


Figure 3.23: Decay scheme of ^{137}Cs (with the use of [2]).

Again the ^{137}Cs source is placed outside on the middle-left of the TPC, and 10^7 events or ^{137}Cs particles are simulated. The simulated spectrum of ^{137}Cs can also be obtained from the deposited energy in the TPC as described before.

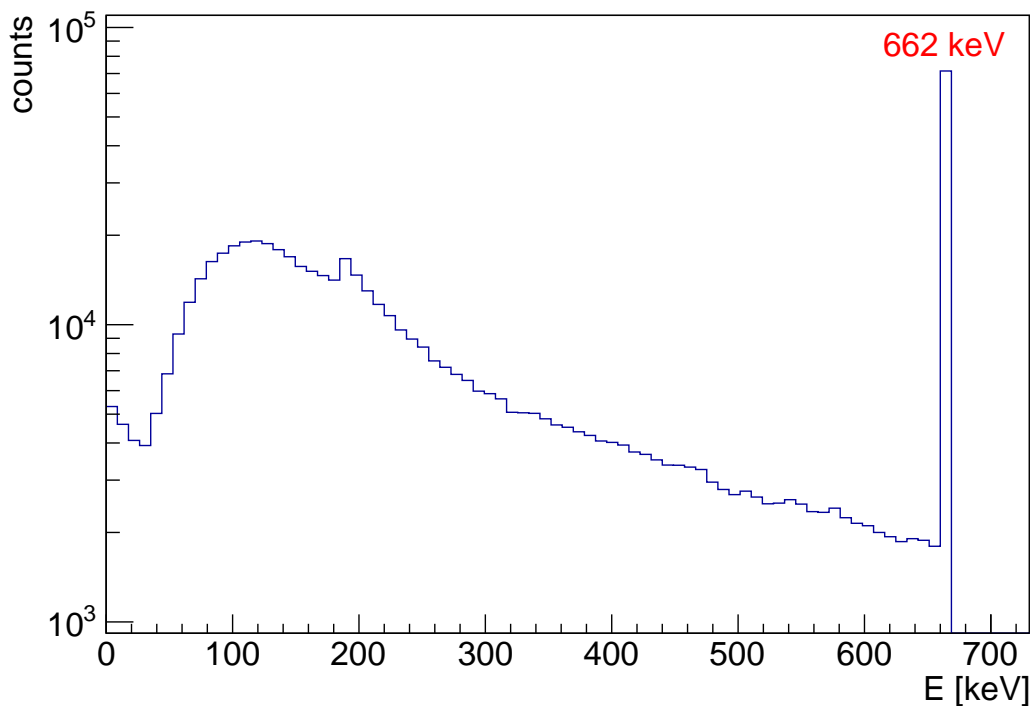


Figure 3.24: Simulated spectrum of ^{137}Cs , placed outside the TPC at position $(0, -150, 84.5)$, taken out of the deposited energy.

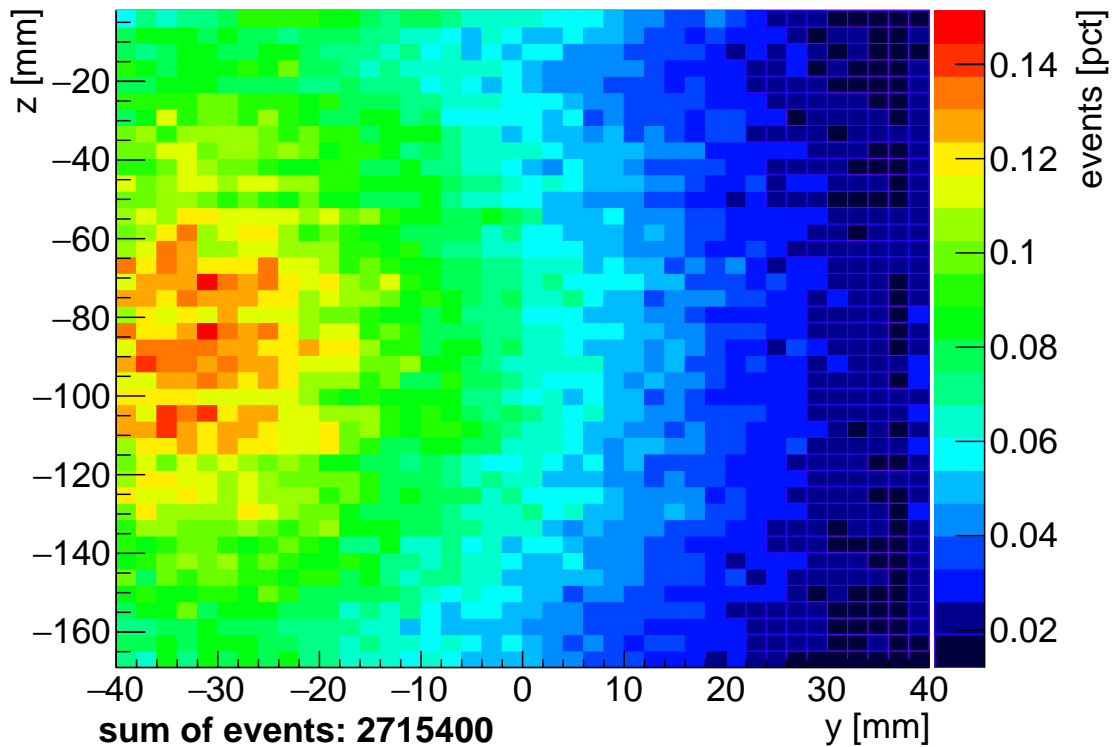
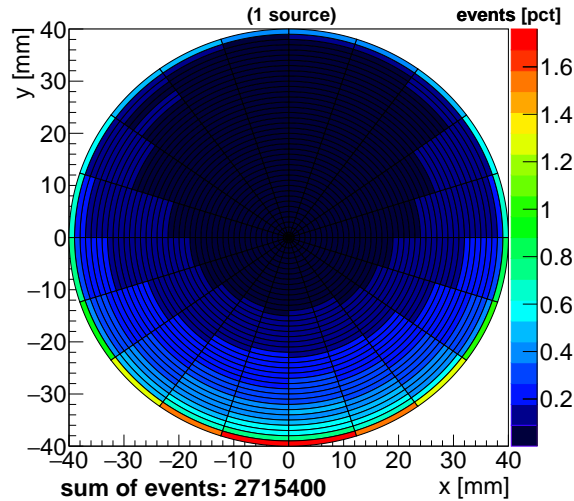


Figure 3.25: Position of events or interactions in the Muenster TPC for ^{137}Cs , placed outside the TPC at position $(0, -150, 84.5)$. The simulation is processed with 10^7 ^{137}Cs events, a liquid xenon absorption length of 20 cm and a PTFE reflectivity of 95 %.

As expected, the spectrum exhibits a 662 keV peak and a broader part below the full energy peak, which results from Compton scattering as described before. This also verifies the implementation of ^{137}Cs and the simulation package. In order to compare the ^{137}Cs source to ^{60}Co , a map of the event positions in the detection volume needs to be obtained. Therefore, the values of the z axis are presented as the percentage of the volume of the total amount of events, which is 2715400. The distribution of the events in the liquid xenon volume, which can be seen in figure 3.25, is similar to the distribution for ^{60}Co (figure 3.20), but for ^{137}Cs does not reach the edges of the TPC in z-position placed only at the center position. However an optimal gamma source reaches the TPC in z-position up to $y = 0$. This means that the ^{137}Cs needs to be shifted along the z-axis additionally to the rotation around the TPC. Furthermore, the amount of events in the liquid xenon is much higher for ^{60}Co as for ^{137}Cs . The belonging xy-map is determined and shown in figure 3.26.

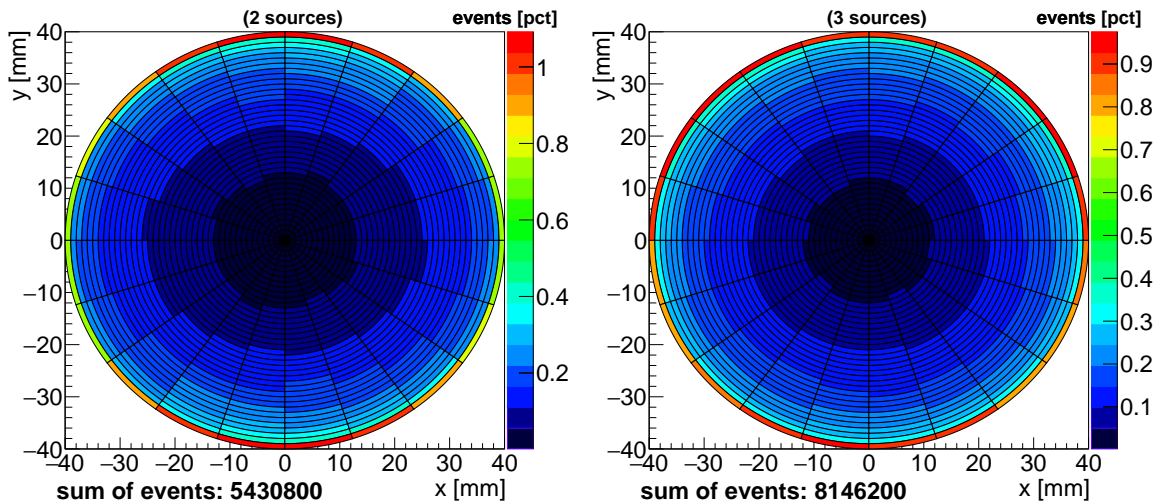
The event distribution in figure 3.26 is unsymmetrical and therefore can not be used for calibration purposes. The maximum and minimum percentage spread is higher than for ^{60}Co by a factor of 1.3. Consequently, the ^{137}Cs source also has to be placed around the TPC. The setup with two and three positions is implemented in the same way as for ^{60}Co .

As seen in figure 3.27(a), two sources are not enough for a full symmetric calibration of the TPC as the circular deviations range, from 0.2% to 0.6%, differs by the factor of 3. As a consequence 3 calibration positions are recommended.



(a) Position of events or interactions in the muenster time projection chamber.

Figure 3.26: Results of the simulations for ^{137}Cs placed outside the time projection chamber at position $(0, -150, 84.5)$. The simulation is processed with 10^7 ^{137}Cs events, a liquid xenon absorption length of 20 cm and a PTFE reflectivity of 95%.



(a) Results of the simulation of two sources placed opposite to each other.

(b) Results of the simulation of three sources placed uniformly placed around the TPC.

Figure 3.27: ^{137}Cs simulations with different amount of sources. These simulations are processed with 10^7 ^{137}Cs events, a liquid xenon absorption length of 20 cm and a PTFE reflectivity of 95%.

In conclusion, both sources, ^{60}Co and ^{137}Cs , can reach the middle of the detection volume and can thus be used to calibrate the TPC. However ^{60}Co can be used more easily because it does not need a shift in the z direction and triggers many more events in a more uniform distribution. However, both sources can only be used to calibrate the TPC with photons of a energy above 100 keV. Calibrations with lower energies can not be performed by placing sources outside of the TPC, because the resulting photons can not pass the TPC walls. A low energy calibration can also be considered by using ^{83m}Kr , which can be doped into the xenon and excites it, allowing the xenon to decay as described in section 2.1. Therefore, the self shielding of xenon as well as the higher energy of the photons can be neglected.

3.3.4 ^{83m}Kr

The before mentioned calibration sources only allow LY calibrations with energies much higher than the for WIMPs expected energies in the order of keV, which are also used to simulate the LY calculation in section 3.2. However, also a low energy radioactive source, like ^{83m}Kr , can be chosen and introduced to the liquid xenon, which allow a uniformly calibration without self shielding effects of the xenon.

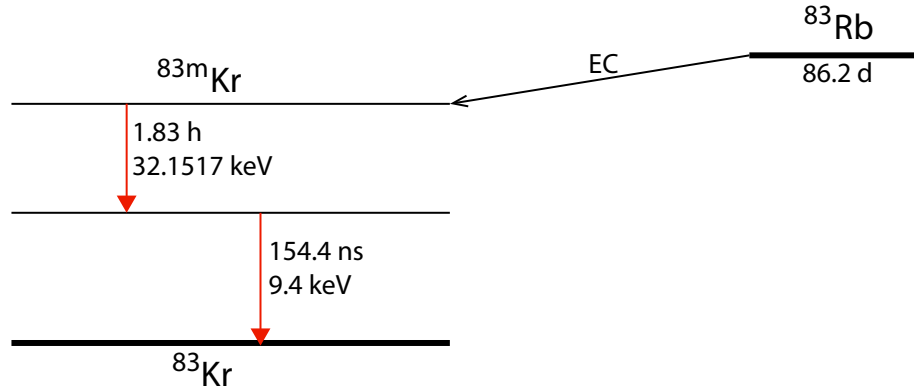


Figure 3.28: Decay scheme of ^{83}Rb and ^{83m}Kr (with the use of [9]).

As can be seen in figure 3.28, ^{83m}Kr has a half-life of 1.83 h, which is long enough to insert it directly in the liquid xenon for calibration measurements and short enough to not contaminate the xenon. This ensures a uniform distribution in the liquid xenon detection volume, which can be verified by obtaining the distribution of the events. Another feature of ^{83m}Kr is the easy handling of the source, which is distributed in pallets that prevents ^{83}Rb to be released. Accordingly 10^7 events or ^{83m}Kr particles are simulated confined to the liquid xenon volume.

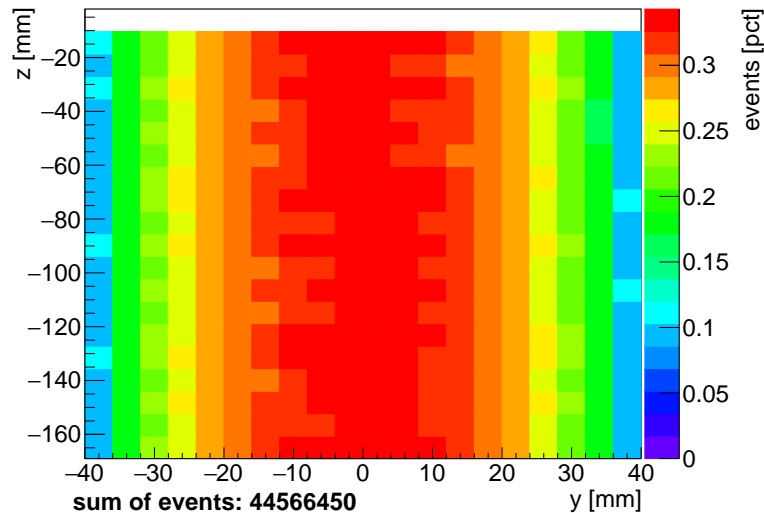


Figure 3.29: Distribution of events in liquid xenon for the ^{83m}Kr simulation.

In figure 3.29 a uniform distribution of events can be observed. Due to the cylindrical shape of the TPC the sum of the events in the zy-plane decreases to the edges. This is another check to see if the simulation package is working properly. Due to the uniform distribution, a LY (see figure 3.30) and a relative LCE (see figure 3.31) can directly determined from the amount of PMT hits of each volume.

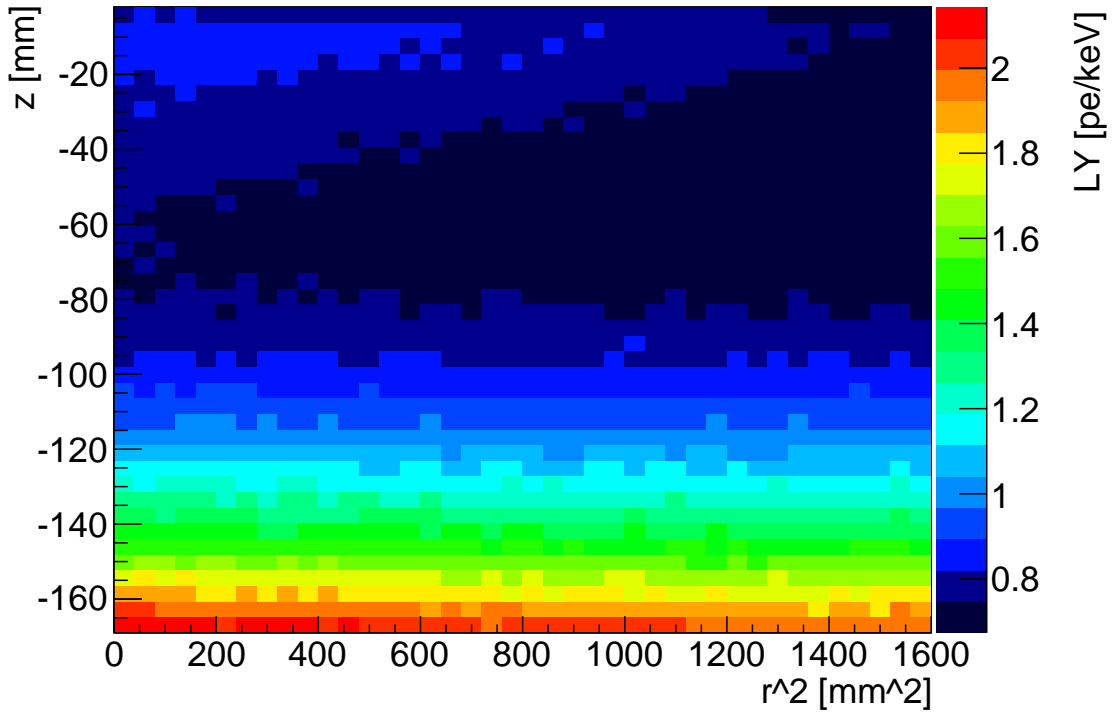


Figure 3.30: Light yield of 10^7 initial ^{83m}Kr events in the Muenster TPC for 1600 volumes. Therefore a average quantum efficiency of 0.3 is assumed. The highest LY value of a single volume corresponds to $1.8 \cdot 10^6$ PMT hits out of it. The simulation is processed with a liquid xenon absorption length of 20 cm and a PTFE reflectivity of 95 %.

The relative LCE seen in figure 3.31 is taken for a liquid xenon absorption length of 20 cm and a reflectivity of 95 %. This relative LCE seems to be equal to the expected LCE, which is simulated with 7 eV optical photons, seen in figure 3.6 and figure 3.8. Therefore, ^{83m}Kr is a good calibration source for doing low energy calibrations with the need of doping the xenon. All in all, three different calibration sources for different calibration scenarios could be obtained. While the commonly used sources for doing calibrations on different energies, ^{60}Co and ^{137}Cs , could be confirmed, ^{83m}Kr , which is used for larger detector setups, also fits perfectly the needs of an optimal calibration source.

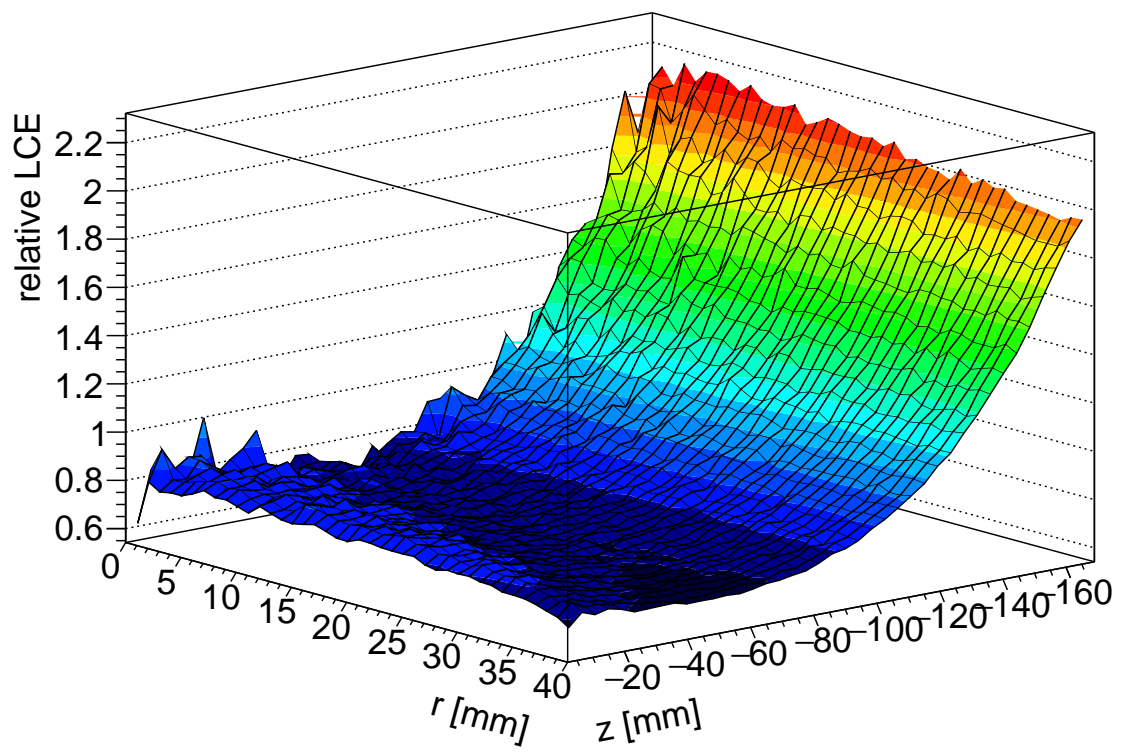


Figure 3.31: Relative LCE of 10^7 simulated ^{83m}Kr events confined to the liquid xenon. Therefore the absorption length of liquid xenon is implemented as 20 cm and the reflectivity of PTFE as 95 %.

4 Conclusion and outlook

Within this bachelor thesis, calibration simulations of the Muenster TPC have been performed. Therefore, the simulation package of the Muenster TPC simulation has been replaced by a updated version, which improves the implementation of low energy physics and paves the way for newer GEANT4 features, such as multi-threading and automatically generated *physicslists*.

With this Monte Carlo based simulation package it is possible to study effects, phenomena and parameters of the Muenster TPC which are necessary for a full understanding of the detector. After some basic tests, which checked the geometrically implementation of the simulated detector setup as well as the implemented physics, the simulation package was used to characterize the Muenster TPC with calibration simulations.

In a first step, the light collection efficiency of the updated simulation package has been obtained and compared to the previous simulation version, as well as the results found in the XENON100 experiment. Therefore, 10^8 optical photons have been simulated in the liquid xenon volume of the TPC, and the amount of detected PMT hits have been determined. The simulations exhibit a huge difference between the two versions of the simulation package. The average LCE of the previous version of the simulation package is 4.59%, while the average LCE of the updated package is obtained as 7.24%. This difference in the simulation packages could be most likely figured out as a different configuration of the refractive index of the grid meshes in the liquid xenon. In the previous version, these meshes were implemented as they would be in gaseous xenon, not in liquid xenon. Since the Muenster TPC experiment is ready for LY studies, the proper configuration will be verified. The relative LCE of the Muenster TPC for an absorption length of 100 cm was also simulated in order to compare it to the relative LCE of XENON100, which is similar to the Muenster TPC. While the relative LCE for the previous simulation version (see figure 3.7) differs widely.

The possibility of performing simulations of a single phase gaseous xenon Muenster TPC has been added and a LCE simulation of this detector setup has been realized. All necessary commands and parameters are implemented to perform calibration simulations with this gaseous xenon TPC for further studies, such as the calibration with ^{83m}Kr , which is ready to be used for the Muenster TPC experiment.

The LCE studies have been expanded to light yield considerations, where the quantum efficiency, the minimum required energy to produce xenon photons and the size of the fraction of the TPC volume is considered. In addition to this, the quantum efficiency could be implemented directly in the simulation package. This would give the possibility to improve the obtained LY, where the quantum efficiency of each PMT must be known, or to measure the quantum efficiency of the PMTs by comparing the LYs. With this implementation, a simulation of the impact of the QE on the LY or LCE of each PMT could also be performed to obtain its importance.

The impact of the absorption length of liquid xenon on the LY as well as the impact of the PTFE reflectivity on the LY are determined. With these relations, it is possible to get the corresponding parameter value of a light yield for the Muenster TPC experiment.

Based on these considerations calibration simulations have been performed to analyze which calibration source fits the needs to obtain a relative LCE of the experimental detector setup. As a result of this, ^{57}Co is excluded, since it could not penetrate the whole TPC. But ^{137}Cs as well as ^{60}Co reach at least the center of the TPC and with a positioning around the TPC it can be used for calibration purposes. While ^{60}Co is only needed to be moved around the TPC, ^{137}Cs also has to be moved to two positions along the z axis. For most calibration purposes, two or three different positions around the TPC are enough. In addition, a fourth non-gamma source has been tested identically. The xenon is doped with ^{83m}Kr , to ensure a calibration of the xenon volumes. The relative LCE, which can be obtained using the LY, is the same as the previously simulated LCE for optical photons confined to the liquid xenon, which underlines the quality of this calibration source. Additionally, to this the self shielding of xenon can be neglected, and therefore ^{83m}Kr is useful for larger xenon volumes.

Up to now, the simulation package can only be used to simulate S1 signals. This could be extended by implementing the electric field of the Muenster TPC, which can be achieved by assigning certain electric field values and shapes to the meshes or copper rings around the TPC. After this, the hit patterns of the S2 signal could be studied and the position reconstruction algorithm of the Muenster TPC experiment as well as the position sensitivity [12] can be investigated. In order to speed up this scintillation based simulations, the multi-threading capabilities of the new GEANT4 version should be used. Therefore, some parts of the simulation package need to be recoded with another programming approach, in which the run of one event is an own process managed by the run management and distributed to accessible processing units.

Bibliography

- [1] geant4.cern.ch, September 2015. 11
- [2] nndc.bnl.gov, September 2015. 26, 29, 33
- [3] physics.nist.gov/physrefdata, September 2015. 8
- [4] E. Aprile. Current status of xenon. talk, 2004. 18
- [5] E. Aprile and T. Doke. Liquid xenon detectors for particle physics and astrophysics. *Reviews of Modern Physics*, 82:2053–2097, July 2010. 3, 4, 5
- [6] L. E. Diaz. Cobalt-57: Uses. JPNM Physics Isotopes, 09 2010. University of Harvard. 26
- [7] E. Aprile et al. The XENON100 dark matter experiment. *Astroparticle Physics*, 35:573–590, April 2012. 6, 7, 16
- [8] C. Levy-Brown. *Studies of Light Propagation And Reflection off of Teflon in Liquid Xenon Detectors in the Context of the XENON100 and XENON1T Dark Matter Experiments*. PhD thesis, WWU Münster, 2014. 8, 9, 12, 16, 18, 27
- [9] Beatrix Ostrick. *Eine kondensierte ^{83m}Kr -Kalibrationsquelle für das KATRIN-Experiment*. PhD thesis, WWU Münster, 2008. 37
- [10] J. Schulz. Design of a 2-phase xenon time projection chamber for electron drift length measurements, 2011. 3
- [11] T. Takahashi, S. Konno, T. Hamada, M. Miyajima, S. Kubota, A. Nakamoto, A. Hitachi, E. Shibamura, and T. Doke. Average energy expended per ion pair in liquid xenon. *Phys. Rev. A*, 12:1771–1775, Nov 1975. 5
- [12] Y. Wei, Q. Lin, X. Xiao, and K. Ni. Study of light detection and sensitivity for a ton-scale liquid xenon dark matter detector. *Journal of Instrumentation*, 8:6002, June 2013. 42